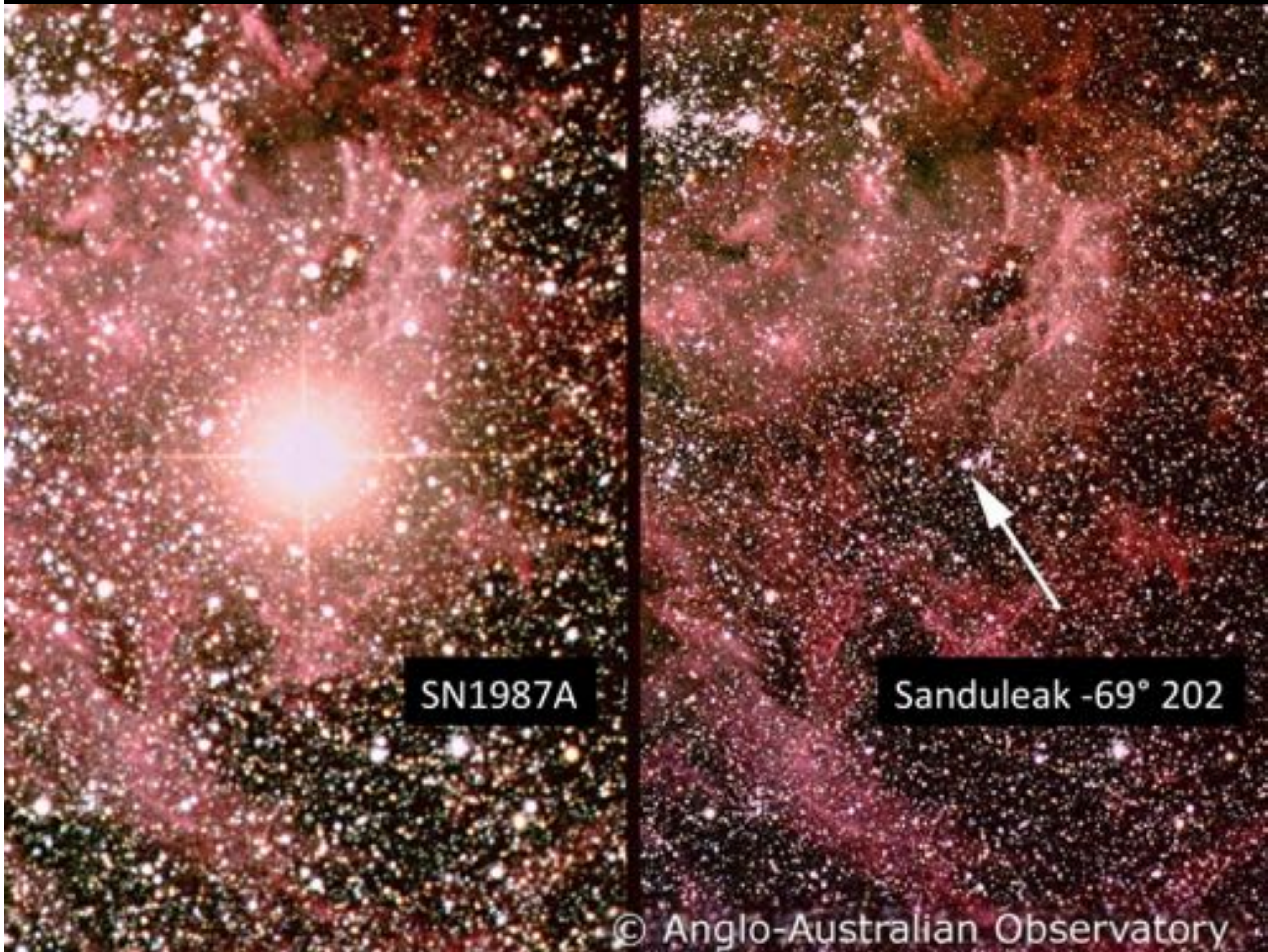

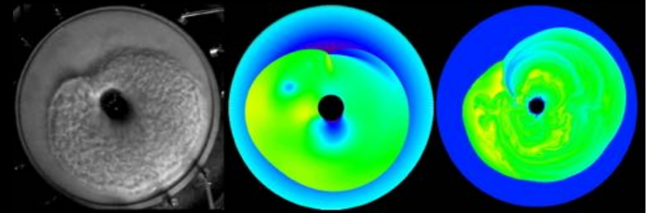

5 lectures on

The Physics of Core-Collapse Supernovae

Outline of lecture 4

The Standing Accretion shock instability

characterization in simulations
linear stability analysis
wave coupling
non linear saturation
shallow water analogue
angular rmomentum budget

Instability of the stationary shock even without neutrino heating

The Standing Accretion Shock Instability has been found in simulations by Blondin+03 using a 2D axisymmetric stationary flow of a perfect gas γ=1.25 with a cooling function

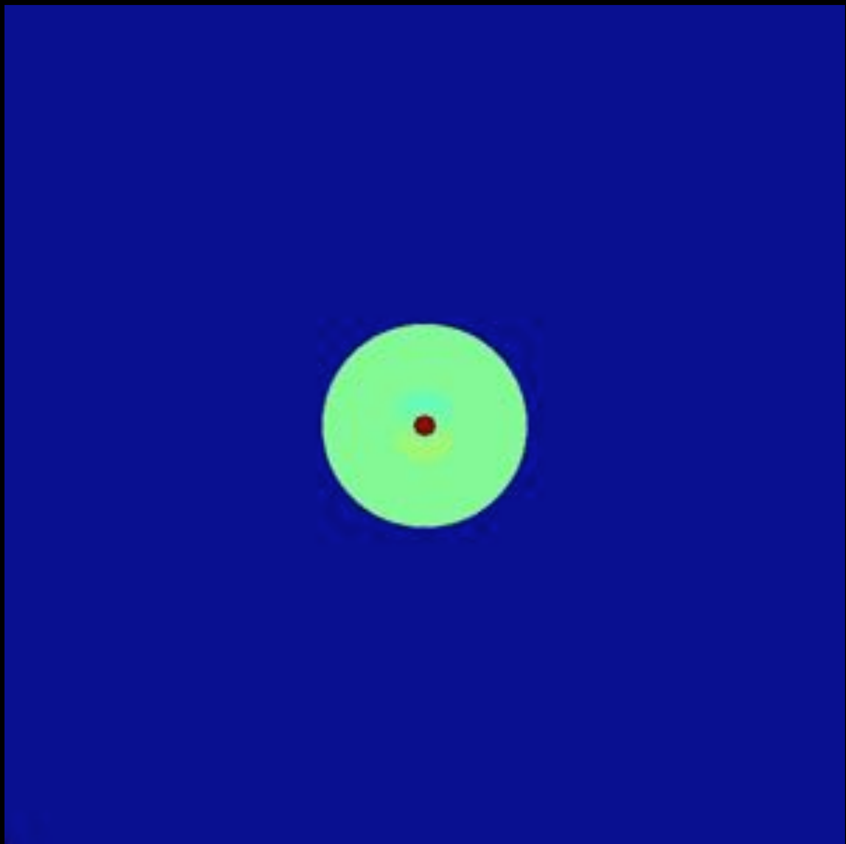

Blondin+03

Blondin+03

The instability SASI in the linear regime is
-dominated by l=1,2 spherical harmonics
-expoential growth with oscillations with a period~30ms

By contrast, neutrino-driven convection is
-dominated by smaller angular scales l=5,6
-exponential growth without oscillations

The mechanism has been identified as the interplay of advected and acoustic perturbations

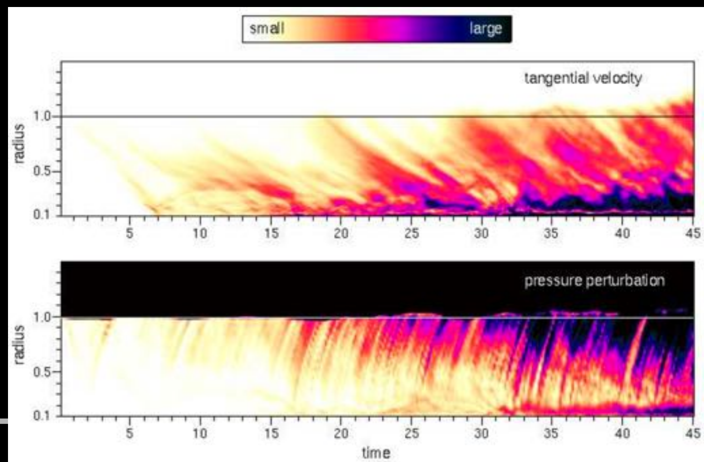

Blondin+03

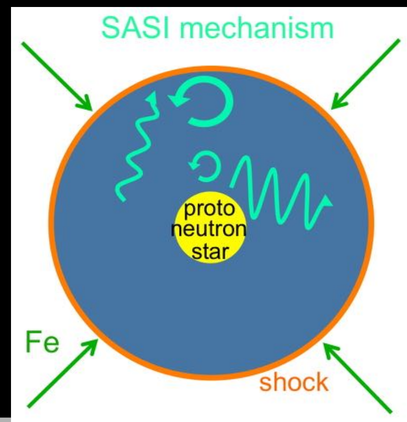

Advective-acoustic cycle in simplified simulations of core-collapse

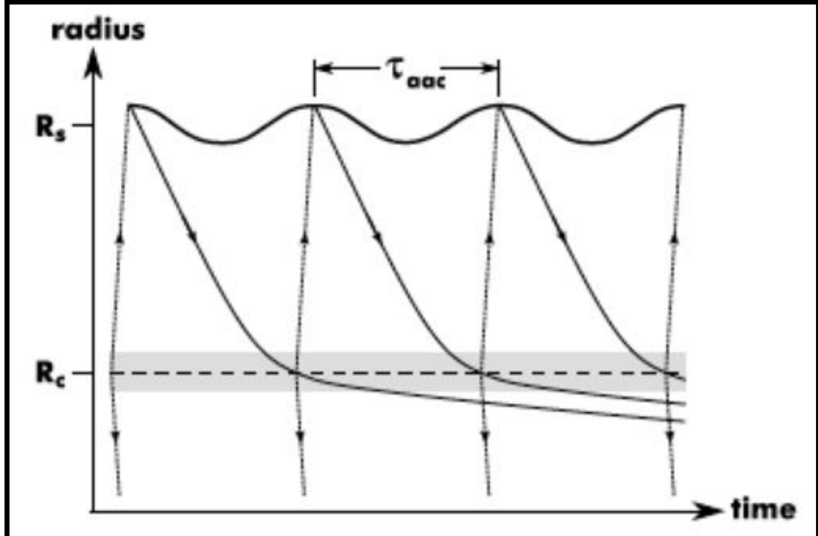

Scheck+08

The feedback region of dominant advective-acoustic coupling is identified as the radius of deceleration R_∇ where the velocity gradients are strongest

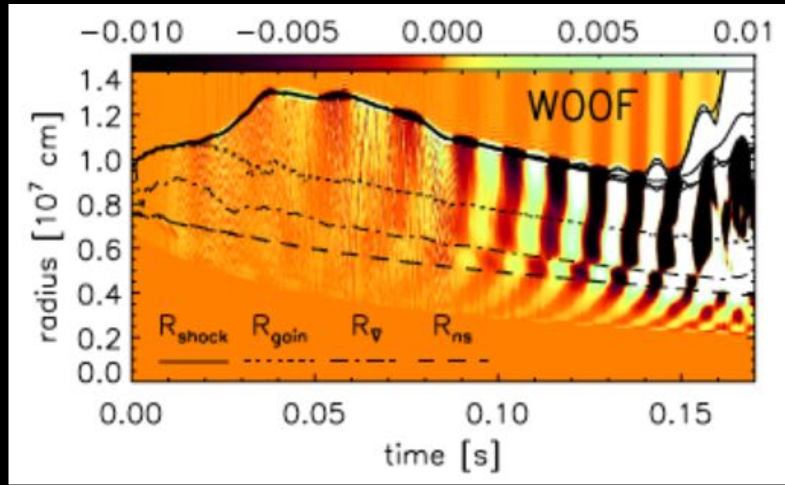

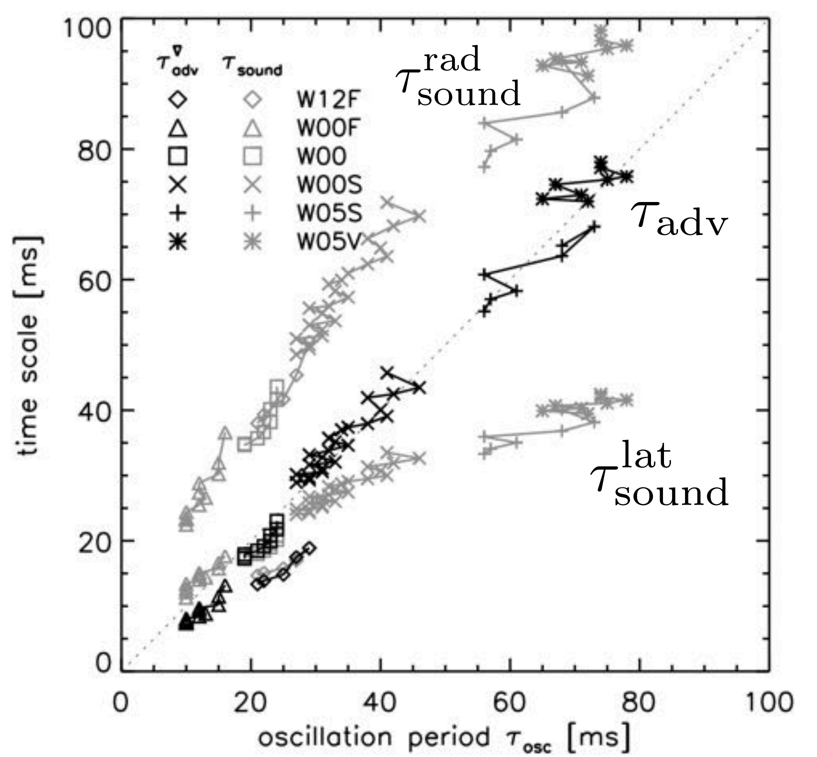

The timescale of the oscillation is better correlated with the advection timescale τ_{adv} than with the sound crossing times, either radial τ^{rad}_{sound} or azimuthal τ^{lat}_{sound}

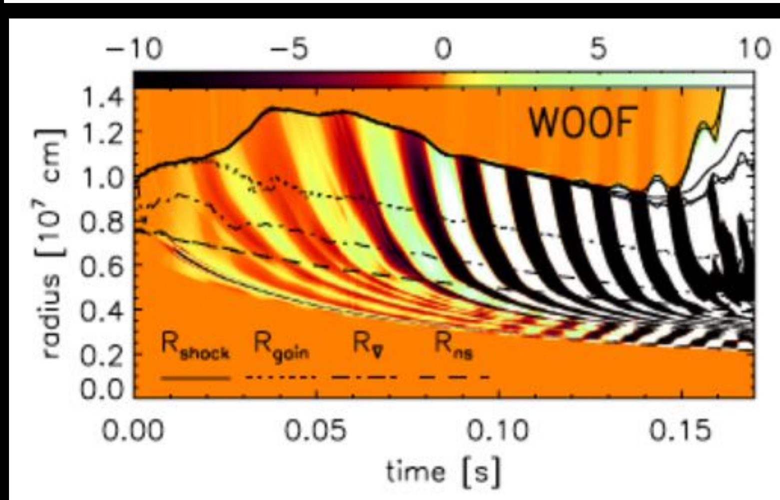

Scheck+08

$$\tau_{adv} \equiv \int_\nabla^{sh} \frac{dr}{v}$$

$$\tau^{rad}_{sound} \equiv 2\left(\int^{sh} \frac{dr}{c-v} + \int^{sh} \frac{dr}{c+v}\right)$$

$$\tau^{lat}_{sound} \equiv \frac{2\pi R_{sh}}{c_{sh}}$$

Should we trust the simulations of SASI ?

Validation of the simulations of SASI in the linear regime
(Blondin & Mezzacappa 06, Foglizzo+07, Fernandez & Thompson 09)

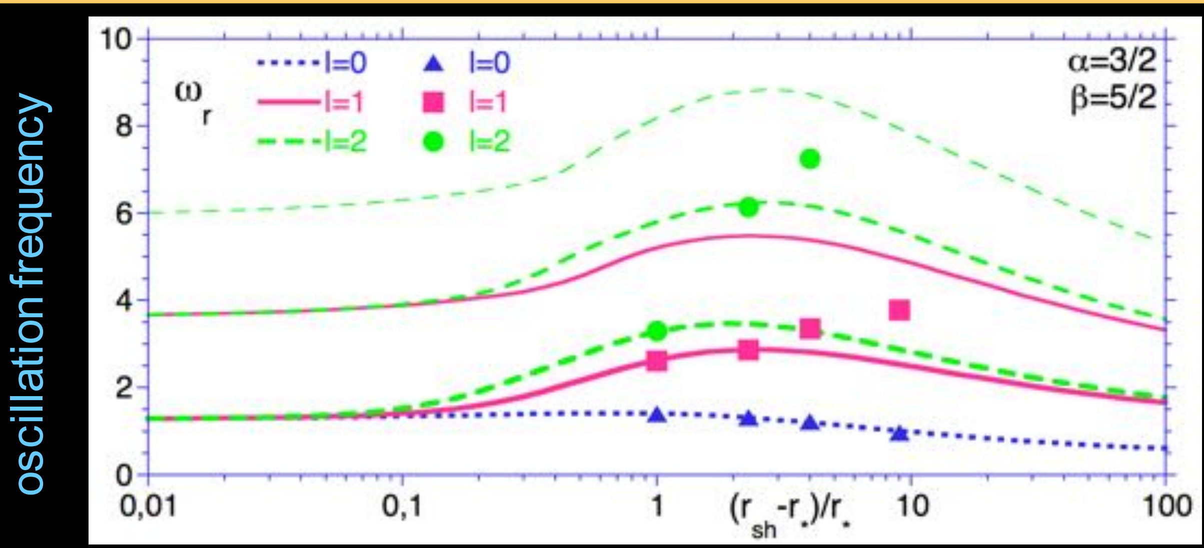

Foglizzo+07

Comparing the eigenfrequencies to the perturbative approach is a good test of the minimum numerical resolution required for the linear stage.

The non linear stage can involve smaller scales and turbulence which can be difficult to capture numerically

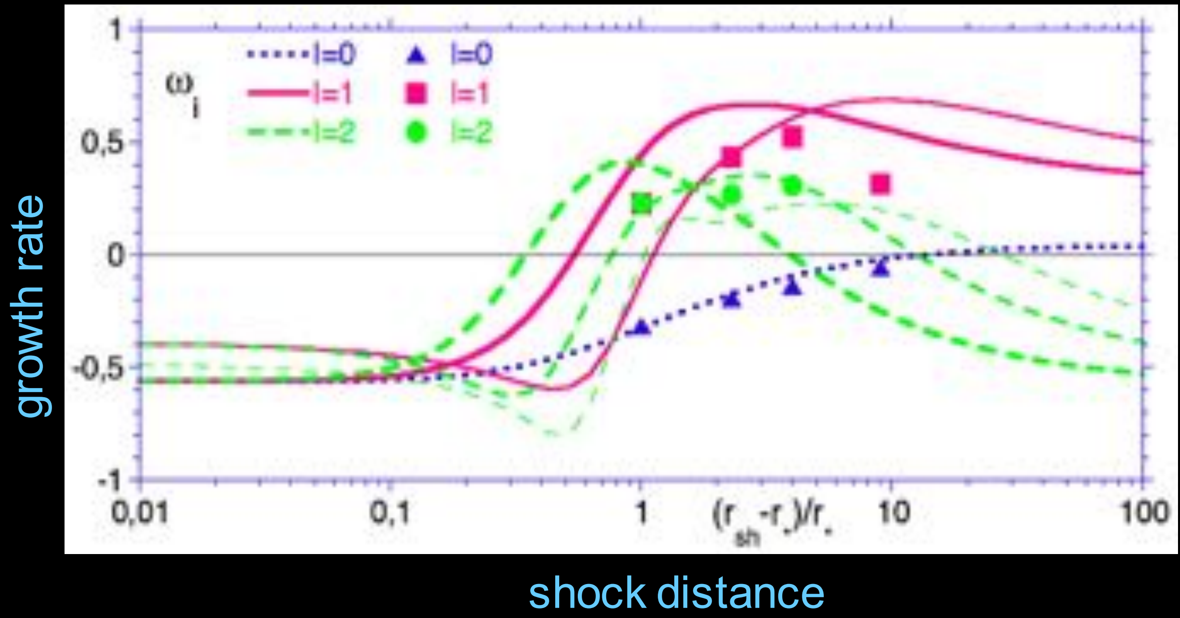

Physical interpretation of the eigenspectrum using wave properties

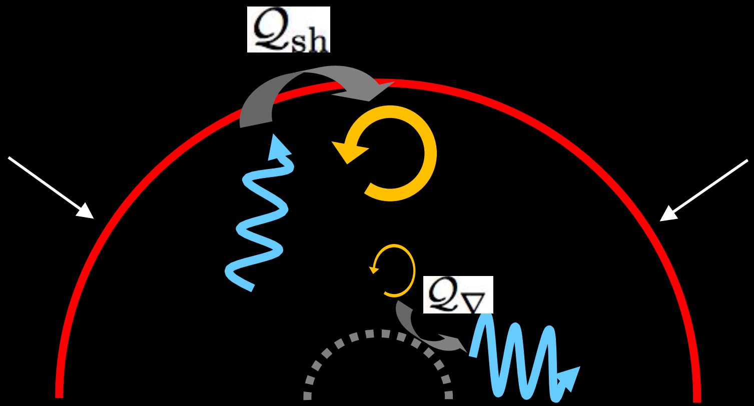

The calculation of the eigenspectrum solves a differential system with a discrete set of complex eigenfrequency.

It does not provide a physical explanantion

The calculation of wave properties and interactions relies on a differential system with a purely real frequency.

It requires additional approximations compared to the calculation of the eigenspectrum

-adiabatic approximation if possible, above the cooling layer and below the gain region

-WKB approximation except in coupling regions

-small growth rate compared to the oscillation frequency

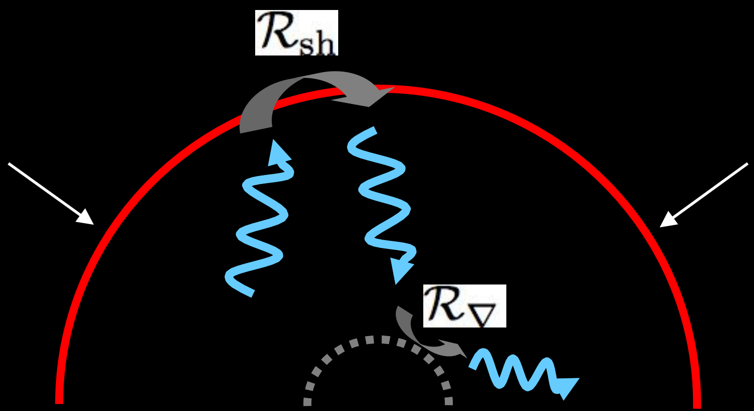

These differences are best viewed in the analysis of the spherical model and plane parallel toy model (Foglizzo 09)

Advective-acoustic cycle in a decelerated, cooled flow

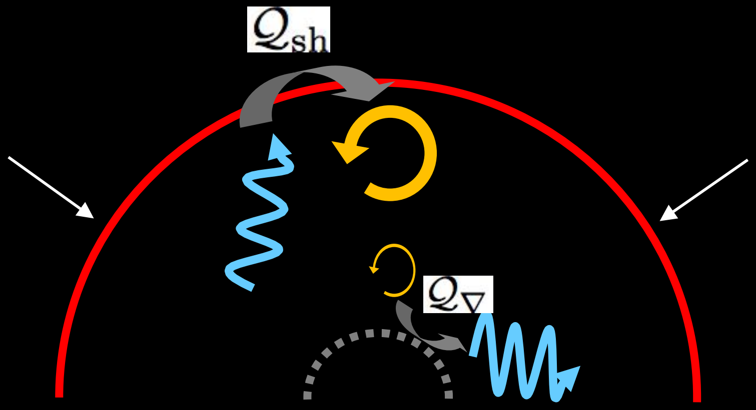

Unstable advective-acoustic cycle Q>1
Stable acoustic cycle R<1

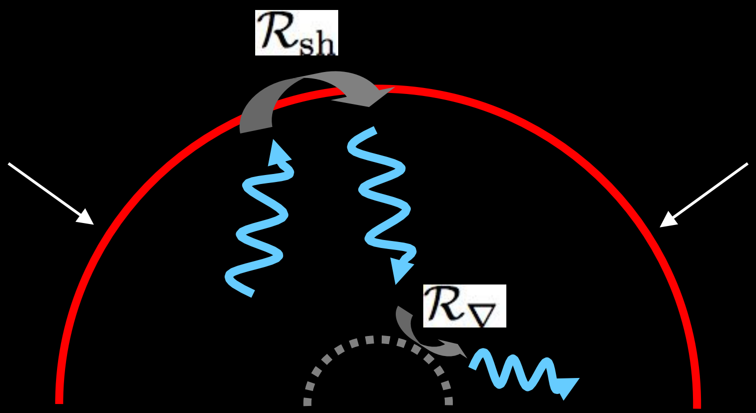

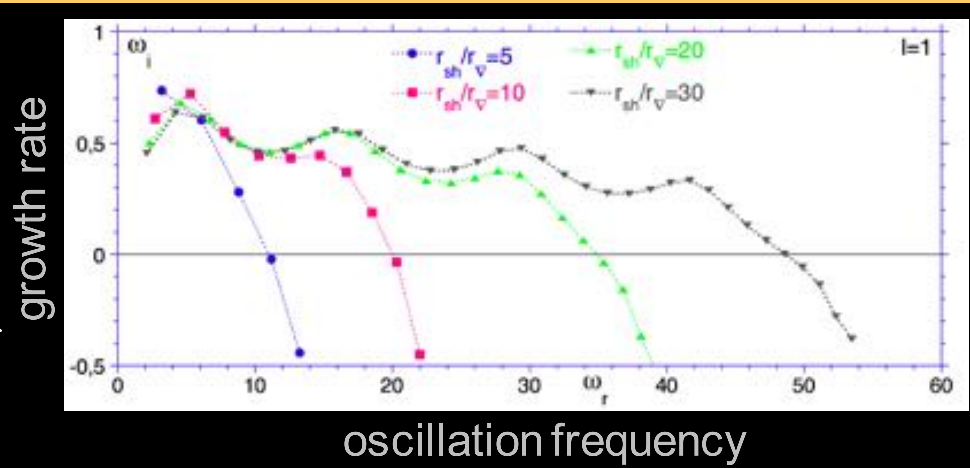

The oscillations $\omega_i(\omega_r)$ are the consequence of interferences between the advective-acoustic and the purely acoustic cyles

The cycle efficiencies $Q(\omega)$, $R(\omega)$ can be deduced from the oscillations $\omega_i(\omega_r)$, or computed in the WKB limit which requires $r_{sh} >> r_\nabla$ (Foglizzo+07). The two cycles can also be discriminated using the frequency spacing of their harmonics (Guilet & Foglizzo 12)

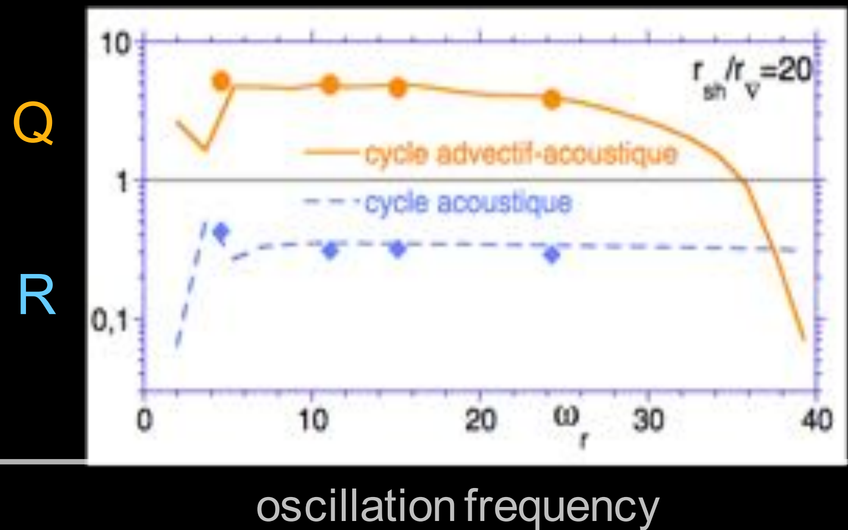

The instability mechanism for a small shock radius is extrapolated from the mechanism revealed by the WKB analysis for a larger radius

Interaction of advected and acoustic perturbations

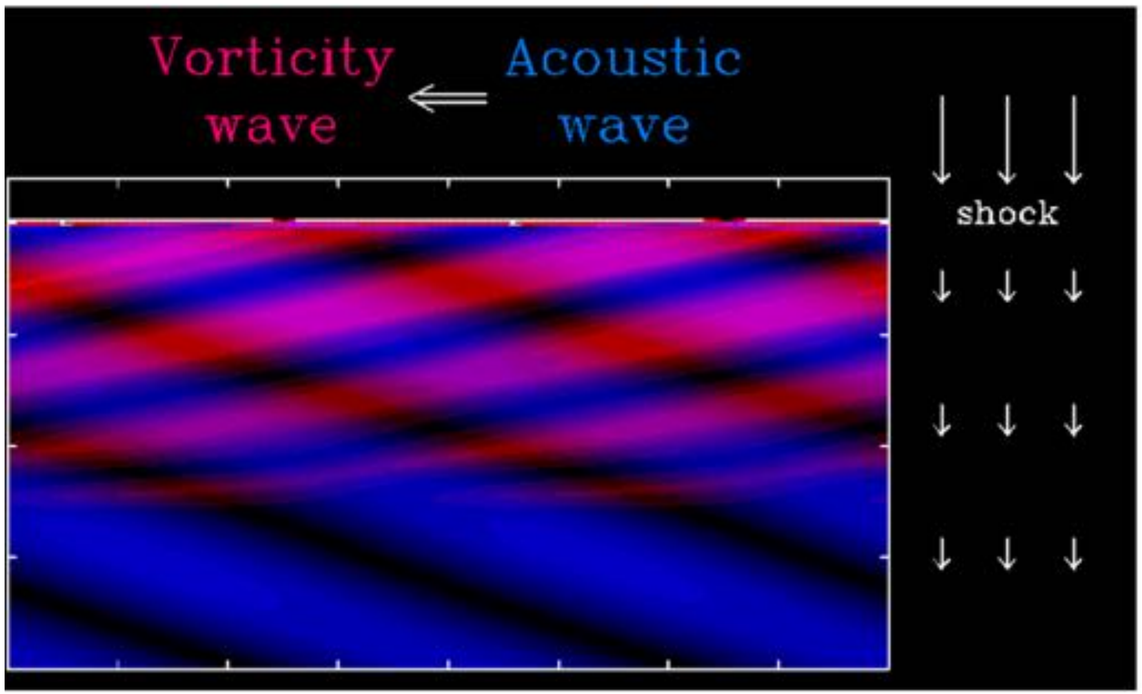

Sato+09

In a uniform stationary flow, advected and acoustic perturbations ignore each other.

If the stationary flow involves gradients, these perturbations are linearly coupled

The advected perturbations δS and δK are source terms in the acoustic equation

$$\frac{\partial^2}{\partial r^2}\frac{\delta p}{p} + a_1\frac{\partial}{\partial r}\frac{\delta p}{p} + a_0\frac{\delta p}{p} = b_0\delta S_{\rm R} + b_1\delta K_{\rm R}.$$

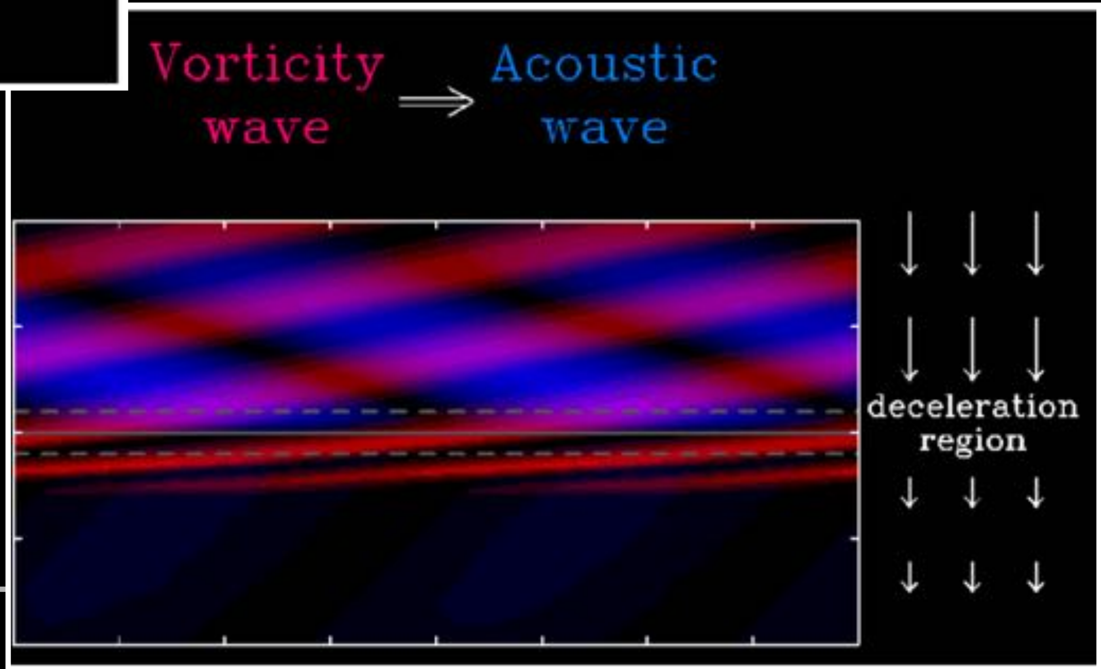

Interaction of advected and acoustic perturbations

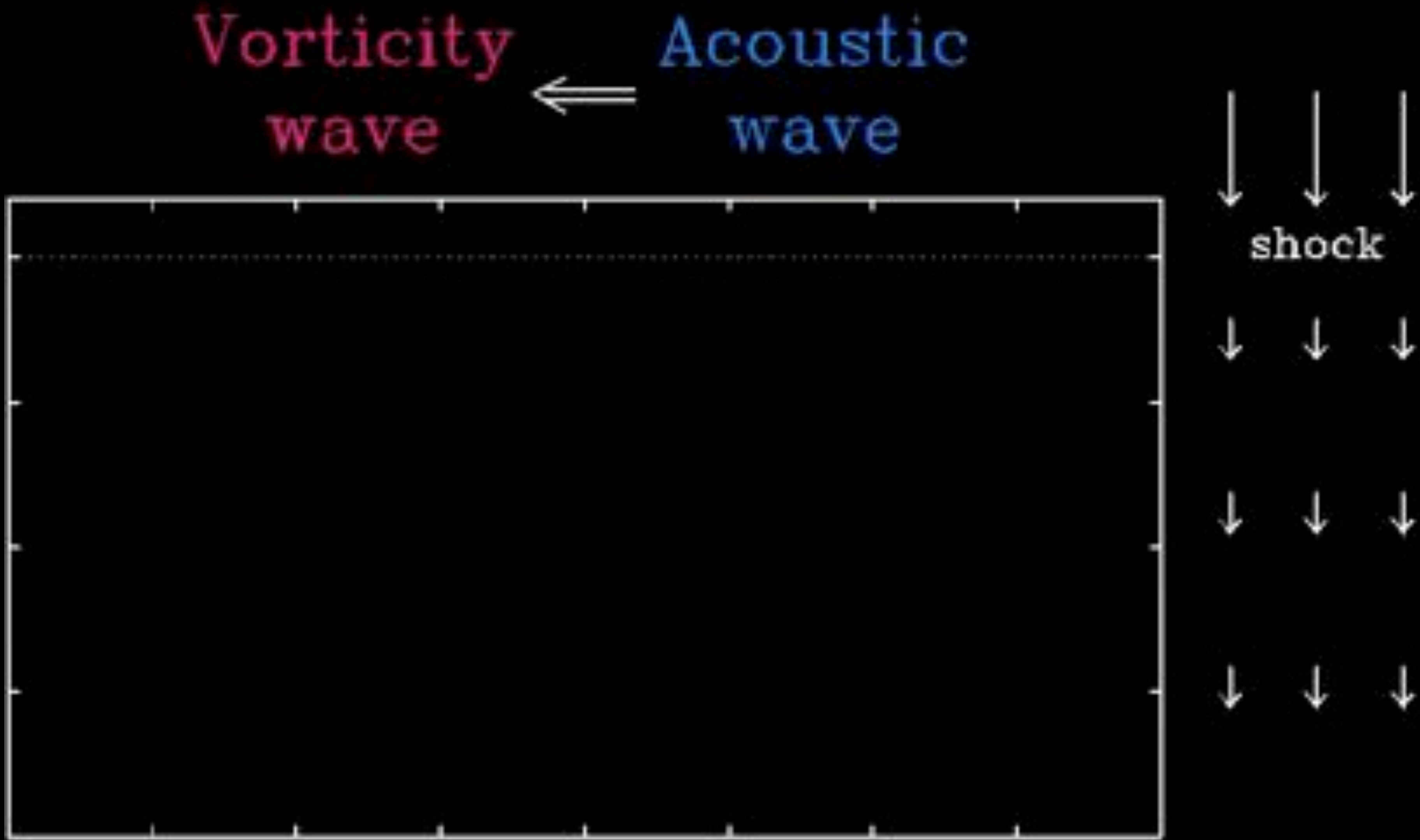

Interaction of advected and acoustic perturbations

Both entropic-acoustic and vortical-acoustic linear couplings can be understood intuitively

advection of entropy

↓

« entropic-acoustic » cycle

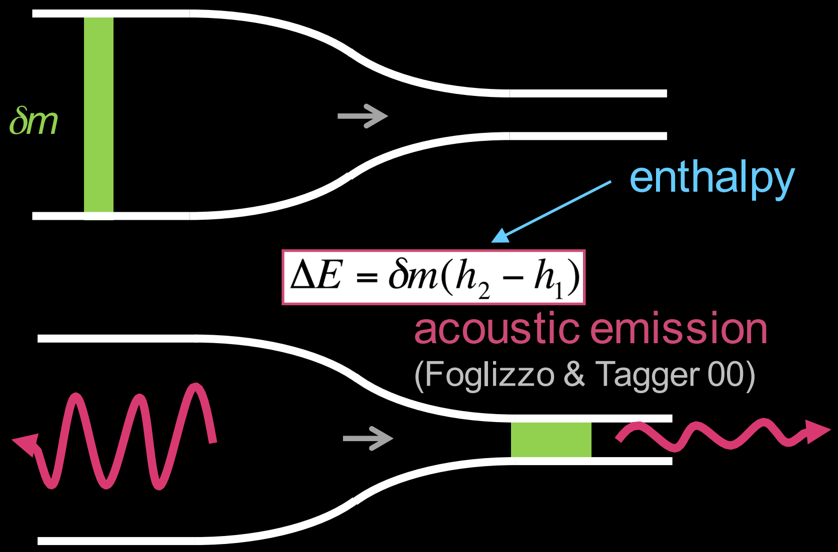

The expansion of a gas upon an adiabatic change of pressure depends on its entropy. Acoustic emission compensates for the change of advected energy: it is proportional to the enthalpy variation in the stationary flow.

advection of vorticity

↓

« vortical-acoustic » cycle

An advected vorticity perturbation cannot settle without breaking the pressure balance: it lifts up dense regions and push down lighter ones.

Shallow water analogue of the vortical-acoustic coupling

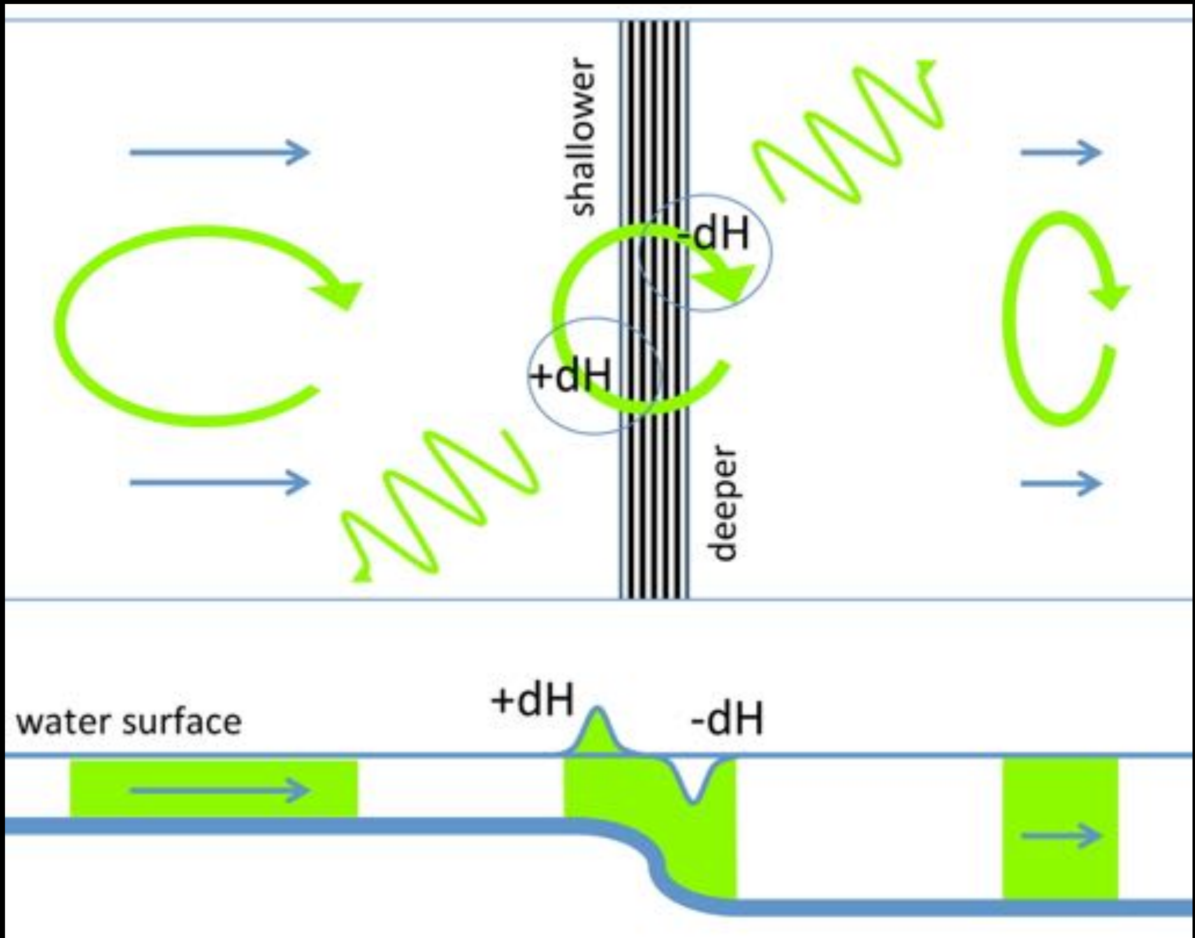

The vortical motion exchanges deep and shallow regions as the perturbation is advected over a change of depth

Aero-acoustic instabilities

- advected perturbations
- acoustic feedback

whistling kettle
Chanaud & Powell 65

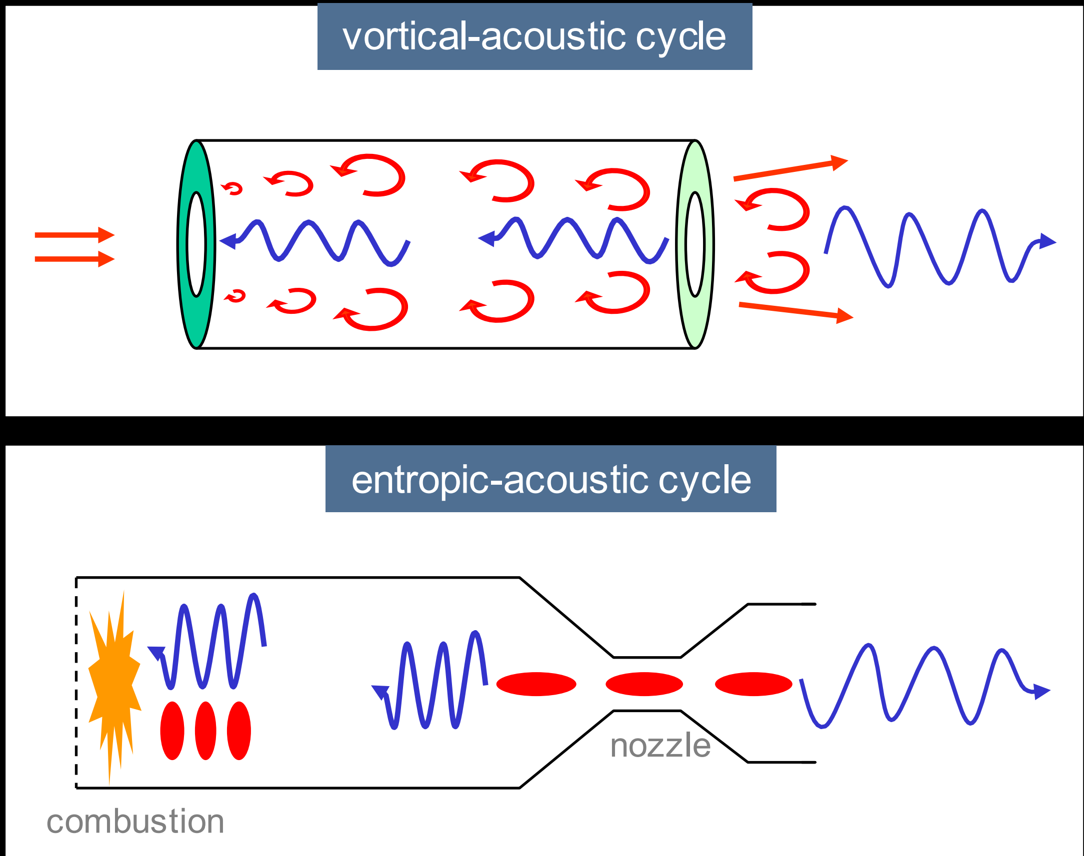

rumble instability of ramjets
Abouseif+84

vibrations
in Ariane 5
Mettenleiter+00

A planar toy model for the advective-acoustic coupling

The planar geometry and uniform flow between the shock and the compact deceleration region allows for a fully analytic calculation

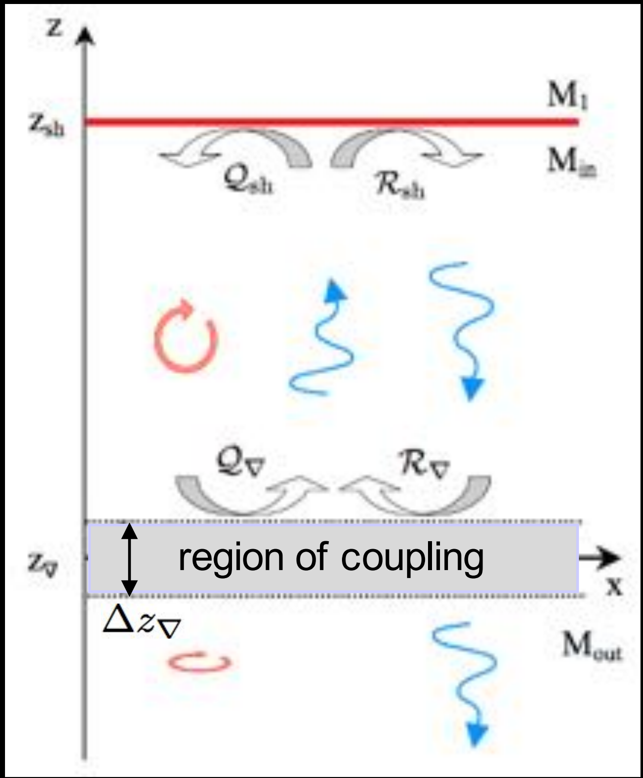

advective-acoustic cycle efficiency $\mathcal{Q} \equiv \mathcal{Q}_{sh}\mathcal{Q}_\nabla$

timescale $\tau_\mathcal{Q}$

purely acoustic cycle efficiency $\mathcal{R} \equiv \mathcal{R}_{sh}\mathcal{R}_\nabla$

timescale $\tau_\mathcal{R}$

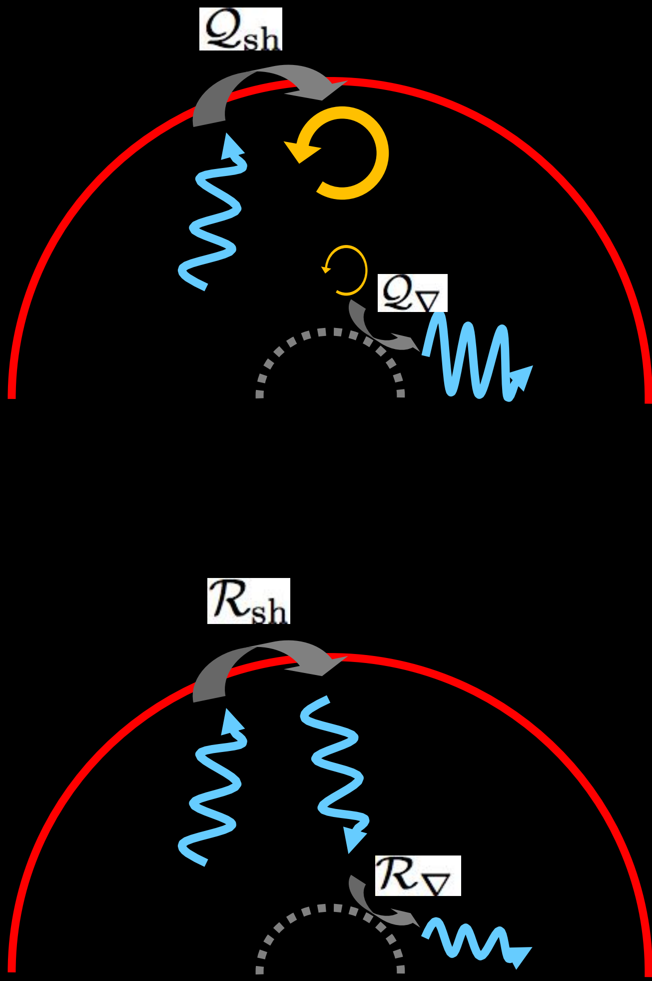

$$\mathcal{Q}e^{i\omega\tau_\mathcal{Q}} + \mathcal{R}e^{i\omega\tau_\mathcal{R}} = 1$$

Explicit analytical expressions for the coupling efficiencies for $\Delta z_\nabla \ll |z_{sh} - z_\nabla|$

A set of complex eigenfrequencies ω satisfy the phase equation relating the two cycles

$$\mathcal{Q}e^{i\omega\tau_{\mathcal{Q}}} + \mathcal{R}e^{i\omega\tau_{\mathcal{R}}} = 1$$

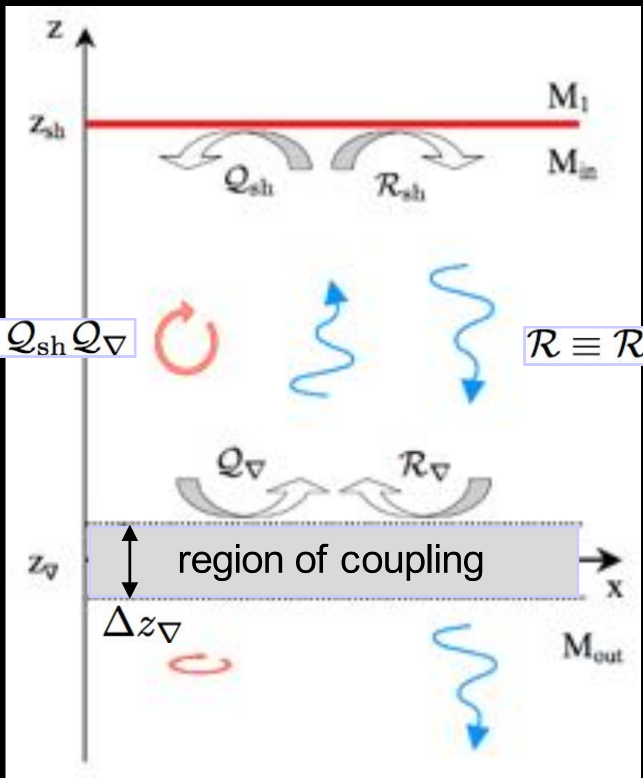

$$\mathcal{Q} \equiv \mathcal{Q}_{\rm sh}\mathcal{Q}_\nabla$$

$$\mathcal{R} \equiv \mathcal{R}_{\rm sh}\mathcal{R}_\nabla$$

Foglizzo 09

$$\mu^2 \equiv 1 - \frac{k_x^2 c^2}{\omega^2}(1-\mathcal{M}^2)$$

The coupling effciencies are defined from the ratio of energy densities δf^-, δf^+, δf_{adv} associated to acoustic and advected perturbations

R_{sh}, Q_{sh} are deduced from the conservation of mass, momentum and energy fluxes across a perturbed shock

$$\mathcal{R}_{\rm sh} \equiv \frac{\delta f_{\rm sh}^+}{\delta f_{\rm sh}^-} = \frac{1+\mu_{\rm sh}\mathcal{M}_{\rm sh}}{1-\mu_{\rm sh}\mathcal{M}_{\rm sh}}\frac{\delta p_{\rm sh}^+}{\delta p_{\rm sh}^-},$$
$$= -\frac{\mu_{\rm sh}^2 - 2\mathcal{M}_{\rm sh}\mu_{\rm sh} + \mathcal{M}_1^{-2}}{\mu_{\rm sh}^2 + 2\mathcal{M}_{\rm sh}\mu_{\rm sh} + \mathcal{M}_1^{-2}}\frac{1+\mu_{\rm sh}\mathcal{M}_{\rm sh}}{1-\mu_{\rm sh}\mathcal{M}_{\rm sh}}.$$

$$\mathcal{Q}_{\rm sh} \equiv \frac{\delta f_{\rm sh}^S}{\delta f_{\rm sh}^-} = \frac{1}{1-\mu_{\rm sh}\mathcal{M}_{\rm sh}}\frac{p_{\rm sh}\delta S_{\rm sh}}{\delta p_{\rm sh}^-},$$
$$= \frac{2}{\mathcal{M}_{\rm sh}}\frac{1-\mathcal{M}_{\rm sh}^2}{1+\gamma\mathcal{M}_{\rm sh}^2}\left(1-\frac{\mathcal{M}_{\rm sh}^2}{\mathcal{M}_1^2}\right)$$
$$\times\frac{\mu_{\rm sh}}{(1-\mu_{\rm sh}\mathcal{M}_{\rm sh})(\mu_{\rm sh}^2+2\mu_{\rm sh}\mathcal{M}_{\rm sh}+\mathcal{M}_1^{-2})},$$

R_∇, Q_∇ are deduced from the conservation of mass and energy fluxes across the compact deceleration region

$$\mathcal{R}_\nabla = \frac{\mu_{\rm in}\mathcal{M}_{\rm out}c_{\rm out}^2 - \mu_{\rm out}\mathcal{M}_{\rm in}c_{\rm in}^2}{\mu_{\rm in}\mathcal{M}_{\rm out}c_{\rm out}^2 + \mu_{\rm out}\mathcal{M}_{\rm in}c_{\rm in}^2}e^{i\omega\tau_{\mathcal{R}}},$$

$$\mathcal{Q}_\nabla = \frac{\mathcal{M}_{\rm out}+\mu_{\rm out}}{1+\mu_{\rm out}\mathcal{M}_{\rm out}}\frac{e^{i\omega\tau_{\mathcal{Q}}}}{\mu_{\rm out}\frac{c_{\rm in}^2}{c_{\rm out}^2}+\mu_{\rm in}\frac{\mathcal{M}_{\rm out}}{\mathcal{M}_{\rm in}}}$$
$$\times\left[1-\frac{c_{\rm in}^2}{c_{\rm out}^2}+\frac{k_x^2 c_{\rm in}^2}{\omega^2}(\mathcal{M}_{\rm in}^2-\mathcal{M}_{\rm out}^2)\right],$$

Efficiency of the advective-acoustic feedback from adiabatic gradients

As a vorticity perturbation δw is advected in a settling flow, the lifting up of dense regions is done at the expense of the kinetic energy of the perturbation. The energy of the acoustic feedback is thus limited by the kinetic energy of the vorticity perturbation.

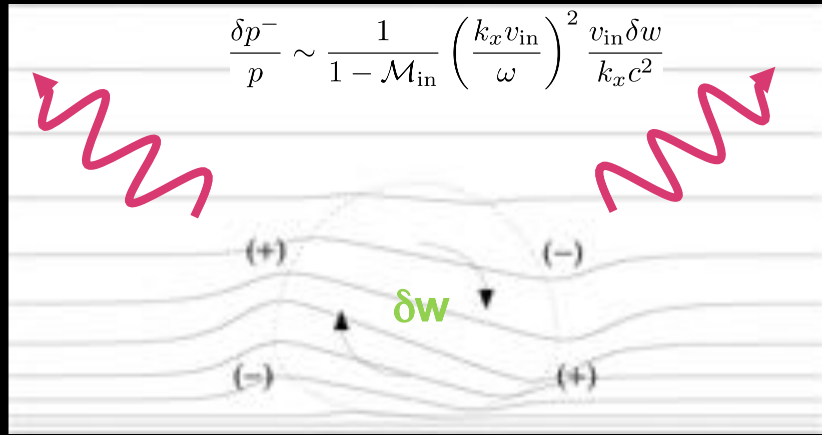

Foglizzo 09

$$Q_\nabla = \frac{\mathcal{M}_{out} + \mu_{out}}{1 + \mu_{out}\mathcal{M}_{out}} \frac{e^{i\omega\tau_Q}}{\mu_{out}\frac{c_{in}^2}{c_{out}^2} + \mu_{in}\frac{\mathcal{M}_{out}}{\mathcal{M}_{in}}} \times \left[1 - \frac{c_{in}^2}{c_{out}^2} + \frac{k_x^2 c_{in}^2}{\omega^2}\left(\mathcal{M}_{in}^2 - \mathcal{M}_{out}^2\right)\right],$$

By contrast the acoustic feedback from the advection of an entropy perturbation can significantly exceed its internal energy: a small entropy perturbation δS can produce a huge acoustic feedback δp^- if the adiabatic increase of enthalpy $(c_{out}/c_{in})^2$ is large enough.

Efficiency of the advective-acoustic coupling

Foglizzo 09

$$
\begin{aligned}
\mathcal{Q}_{\rm sh} \equiv \frac{\delta f^S_{\rm sh}}{\delta f^-_{\rm sh}} &= \frac{1}{1-\mu_{\rm sh}\mathcal{M}_{\rm sh}}\frac{p_{\rm sh}\delta S_{\rm sh}}{\delta p^-_{\rm sh}}, \\
&= \frac{2}{\mathcal{M}_{\rm sh}}\frac{1-\mathcal{M}^2_{\rm sh}}{1+\gamma\mathcal{M}^2_{\rm sh}}\left(1-\frac{\mathcal{M}^2_{\rm sh}}{\mathcal{M}^2_1}\right) \\
&\times \frac{\mu_{\rm sh}}{(1-\mu_{\rm sh}\mathcal{M}_{\rm sh})(\mu^2_{\rm sh}+2\mu_{\rm sh}\mathcal{M}_{\rm sh}+\mathcal{M}_1^{-2})},
\end{aligned}
$$

The production of vorticity and entropy from an acoustic wave reaching the shock can be very large only for a strong shock in the isothermal limit

$$
\rightarrow \quad
\begin{aligned}
|\mathcal{Q}_{\rm sh}| &\sim \frac{1}{\mathcal{M}^2_{\rm sh}}\frac{1-\mathcal{M}^2_{\rm sh}}{1+\gamma\mathcal{M}^2_{\rm sh}} \\
&\sim \mathcal{M}^2_1 \ \text{ if } \ \gamma = 1
\end{aligned}
$$

A strong advective-acoustic cycle $Q = Q_{sh} Q_{\nabla} >>1$ could be fed:

-by a strong vortical-acoustic coupling at the shock $Q_{sh} \sim M_1^2 >>1$
if the shock were isothermal and strong,

-by a strong entropic-acoustic coupling in the feedback region $Q_{\nabla} \sim (\rho_{out}/\rho_{in})^{\gamma-1} >>1$
if the adiabatic compression were large.

The global efficiency is moderate $Q\sim 1\text{-}3$ in the core-collapse accretion flow ($\gamma\sim 4/3$, $M_1\sim 5$, $r_{sh}/r_{\nabla}\sim 2\text{-}4$).

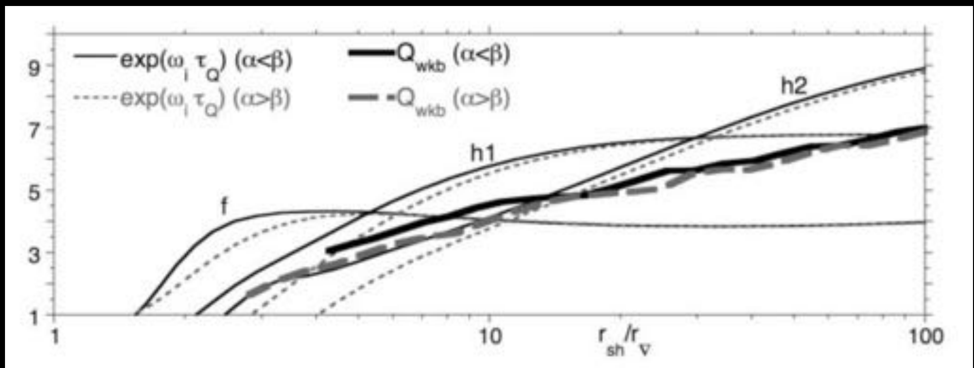

Foglizzo+07

Müller+12

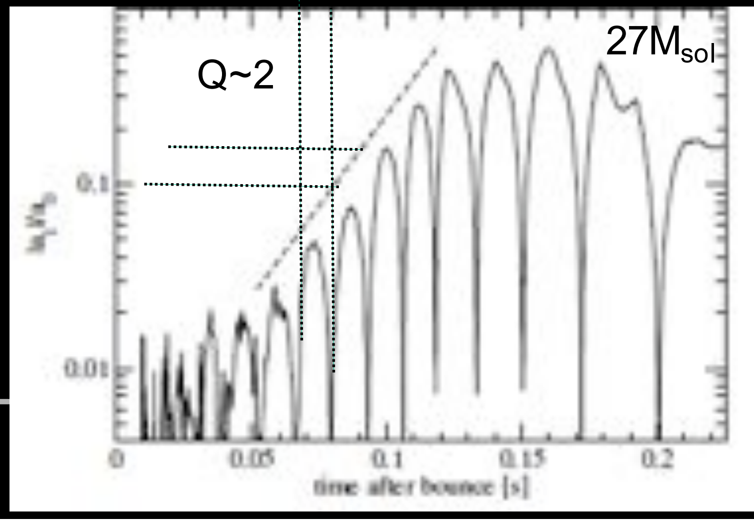

Interferences between the advective-acoustic cycle and the purely acoustic cycle

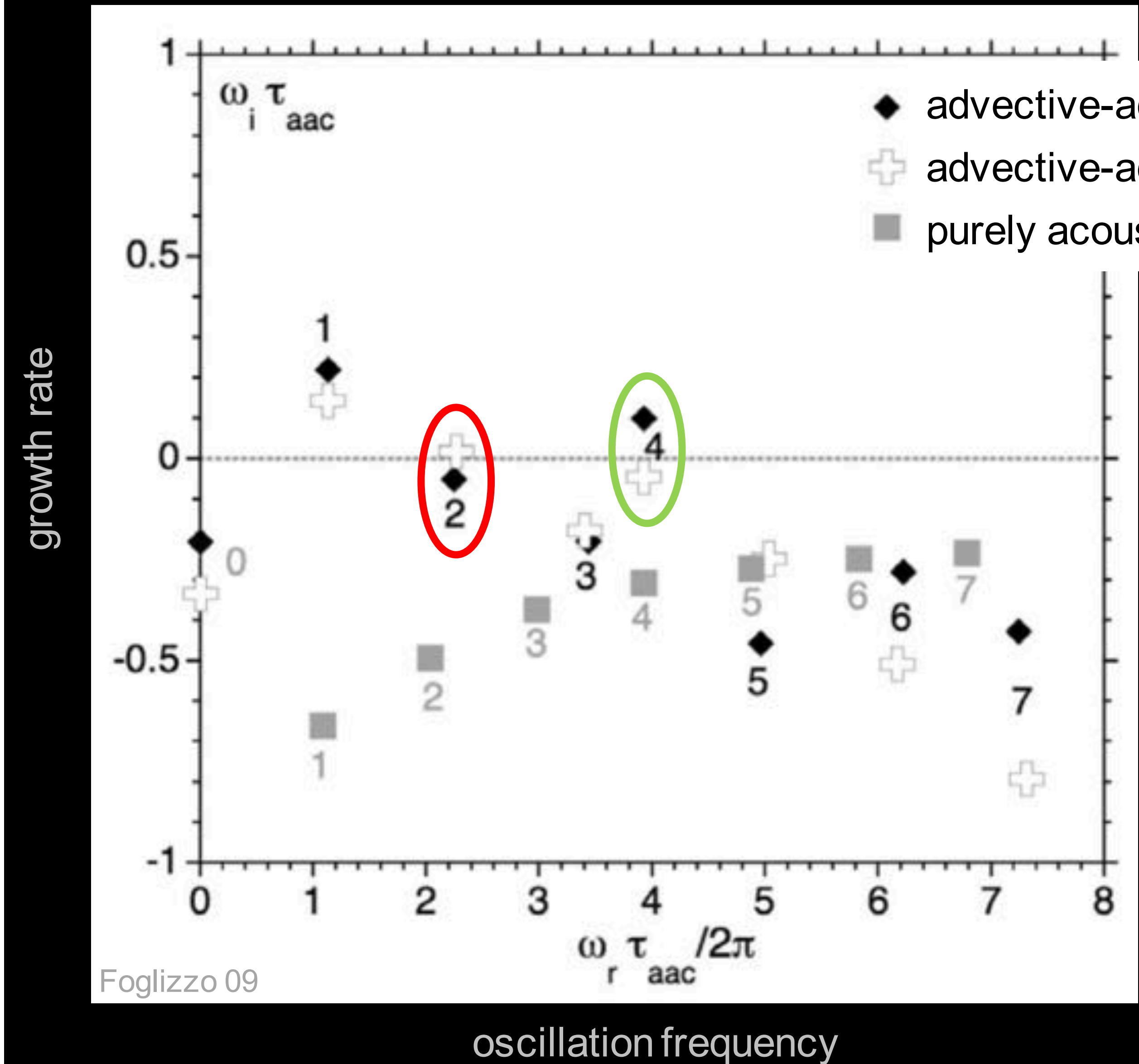

If Q>>1 the advective-acoustic cyle is so strong that the purely acoustic cycle can be neglected. However, the contribution of the purely acoustic cycle can be decisive near marginal stability

In this example, the mode n_x=2 would be unstable with the advective-acoustic cycle alone, but the destructive interference with the purely acoustic cycle makes it stable

Conversely, the mode n_x=4 would be stable with the advective-acoustic cycle alone, but the constructive interference with the purely acoustic cycle makes it unstable

see also Fernandez & Thompson 09

Understanding the efficiency of the acoustic feedback (Foglizzo 09)

$M_1=5$, $\gamma=4/3$, $T_{in}/T_{out}=0.75$

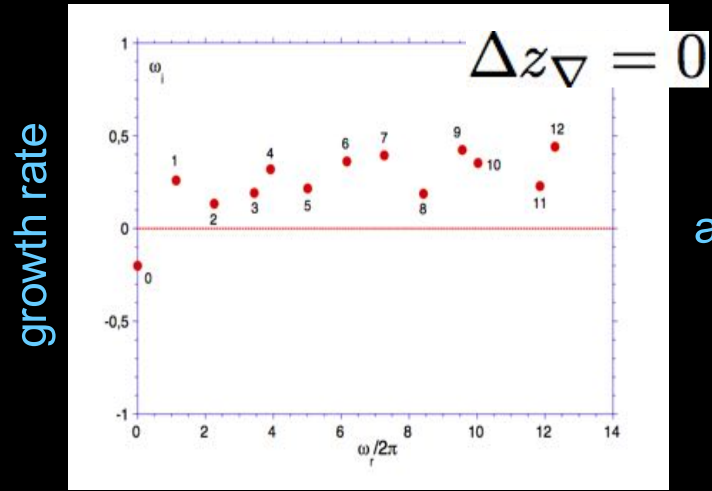

fully analytic

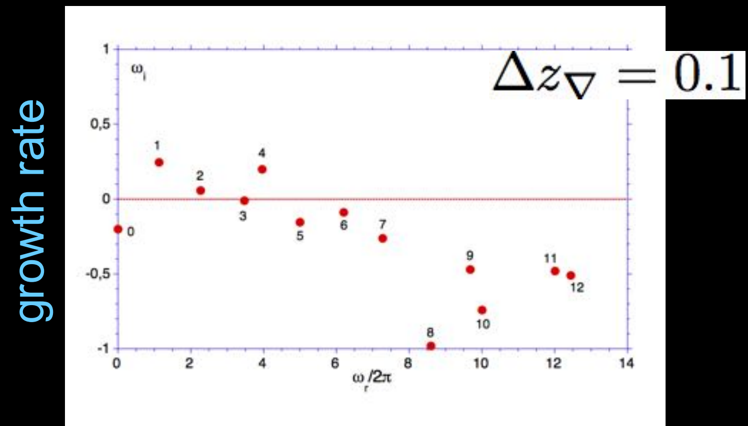

oscillation frequency

The finite lengthscale of the deceleration region introduces a frequency cut-off associated to the crossing time τ_∇

$$\omega_{\rm cut} \sim \frac{1}{\tau_\nabla}.$$

$$Q_\nabla = \int_{\rm bc}^{\rm sh} b_0 \frac{\delta p_0}{p} e^{\int_{\rm sh} \frac{i\omega}{v} {\rm d}z} \frac{\partial b_\nabla}{\partial z} {\rm d}z,$$

where

$$b_0 \equiv \frac{1}{2}\left(1+\frac{k_x^2 v_{\rm sh}^2}{\omega^2}\right)\left(1-\mathcal{R}_\nabla - \frac{1+\mathcal{R}_\nabla}{\mu_{\rm sh}\mathcal{M}_{\rm sh}}\right)$$

$$\frac{1-\mathcal{M}^2}{1-\mathcal{M}_{\rm sh}^2}\frac{\mathcal{M}_{\rm sh}^2}{\mathcal{M}^2}\left(\frac{\delta p_0}{p}\right)_{\rm sh}^{-1} e^{-\int_{\rm sh} \frac{i\omega}{c}\frac{2\mathcal{M}}{1-\mathcal{M}^2}{\rm d}z},$$

$$b_\nabla \equiv \frac{i\omega}{c_{\rm sh}^2}\frac{i\omega - 2v\frac{\partial \log \mathcal{M}}{\partial z}}{k_x^2\mathcal{M}^2 + \frac{\omega^2}{c^2} - v\mathcal{M}^2\frac{\partial}{\partial z}\frac{i\omega}{v^2}}.$$

-high frequency perturbations are stabilized by phase mixing above the cut-off frequency

-high horizontal wavenumber perturbations correspond to higher frequencies. High order overtones produce an evanescent pressure feedback which does not affect the shock

→ SASI is a low frequency instability dominated by l=1,2

The saturation of SASI by parasitic instabilities

Guilet+10

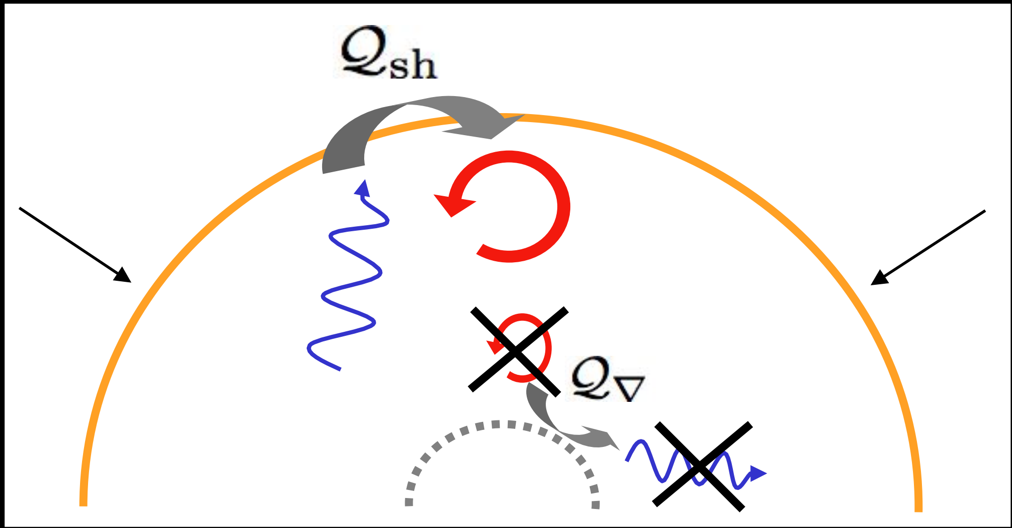

entropy-vorticity wave

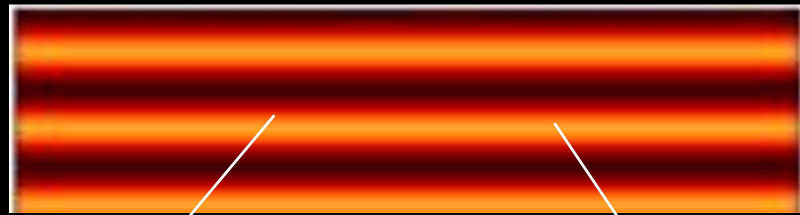

Rayleigh-Taylor

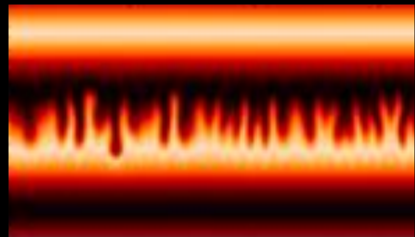

Kelvin-Helmhotz

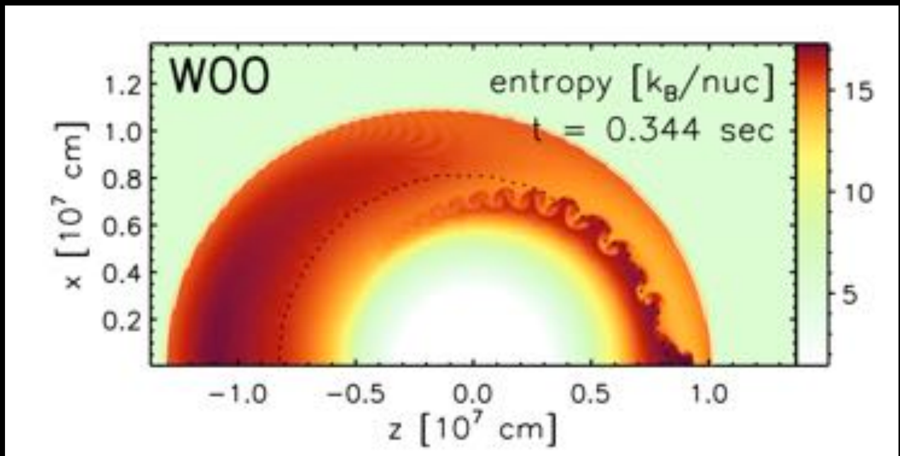

The entropy and vorticity waves produced by the shock oscillations are unstable to parasitic instabilities such as Rayleigh-Taylor and Kelvin-Helmholtz.

The advective-acoustic cycle is affected if

- the parasitic instabilities are able to propagate against the flow,
- their effective eulerian growth rate exceeds the SASI growth rate

Reminder about the Kelvin-Helmholtz instability

Two incompressible fluids with uniform velocities v_1 and v_2

$$\frac{\partial \rho}{\partial t} + \nabla \cdot \rho v = 0,$$
$$\frac{\partial v}{\partial t} + (v \cdot \nabla) v + \frac{\nabla P}{\rho} = 0.$$

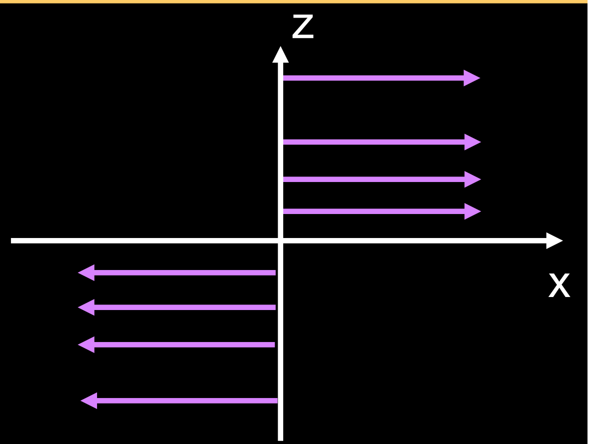

Linearizing, + Fourier transform in time and space: $\exp(-i\omega t + i k_x x + i k_z z)$

$$ik \cdot \delta v = 0,$$
$$-i(\omega - k_x v)\delta v + ik\frac{\delta P}{\rho} = 0.$$

$\rightarrow$ $k^2 \frac{\delta P}{\rho} = 0$ $\rightarrow$ $k_x^2 + k_z^2 = 0$ $\rightarrow$ $k_z = \pm i k_x$

$$k_x \delta v_x + k_z \delta v_z = 0,$$
$$(\omega - k_x v)\delta v_x = k_x \frac{\delta P}{\rho},$$
$$(\omega - k_x v)\delta v_z = k_z \frac{\delta P}{\rho}.$$

$\rightarrow$

$$\delta v_z = -i(\omega - k_x v)\ \delta\zeta\ \mathrm{e}^{-k_x|z|}\mathrm{e}^{ik_x x},$$
$$\delta v_x = \mp(\omega - k_x v)\ \delta\zeta\ \mathrm{e}^{-k_x|z|}\mathrm{e}^{ik_x x},$$
$$\delta P = \pm\frac{(\omega - k_x v)^2}{k_x}\rho\ \delta\zeta\ \mathrm{e}^{-k_x|z|}\mathrm{e}^{ik_x x}.$$

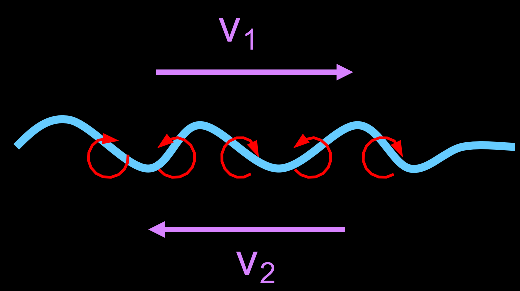

Boundary condition: continuity of the interface pressure δP at $z = \delta\zeta$

$\delta P_1 = \delta P_2$ $\rightarrow$ $\omega = \frac{k_x}{2}(v_1 + v_2 + i|v_1 - v_2|)$

for a step like velocity profile, the most unstable wavelengths are at the smallest scale

Reminder about the Kelvin-Helmholtz instability

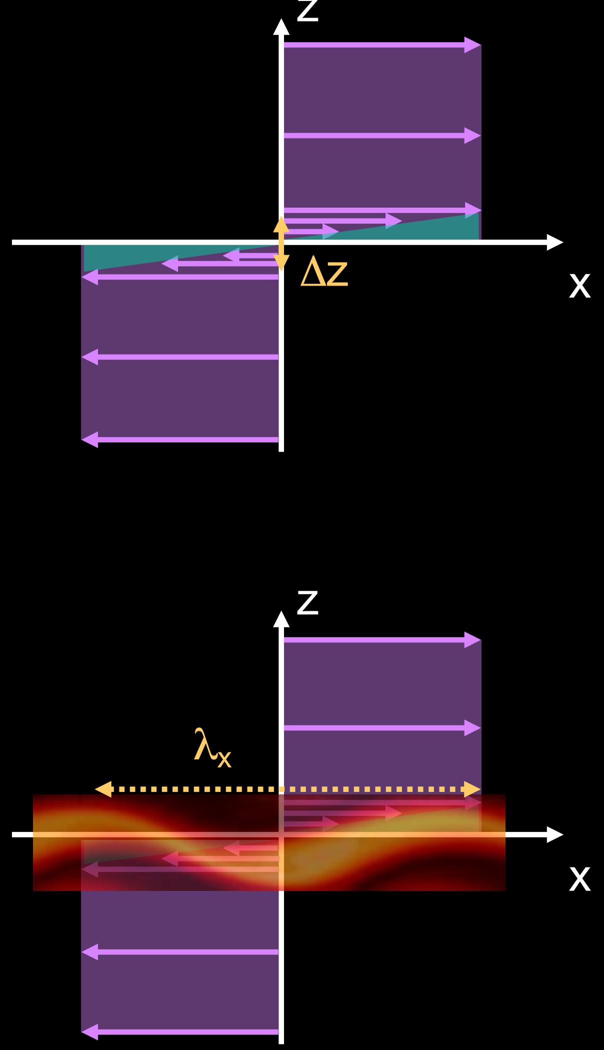

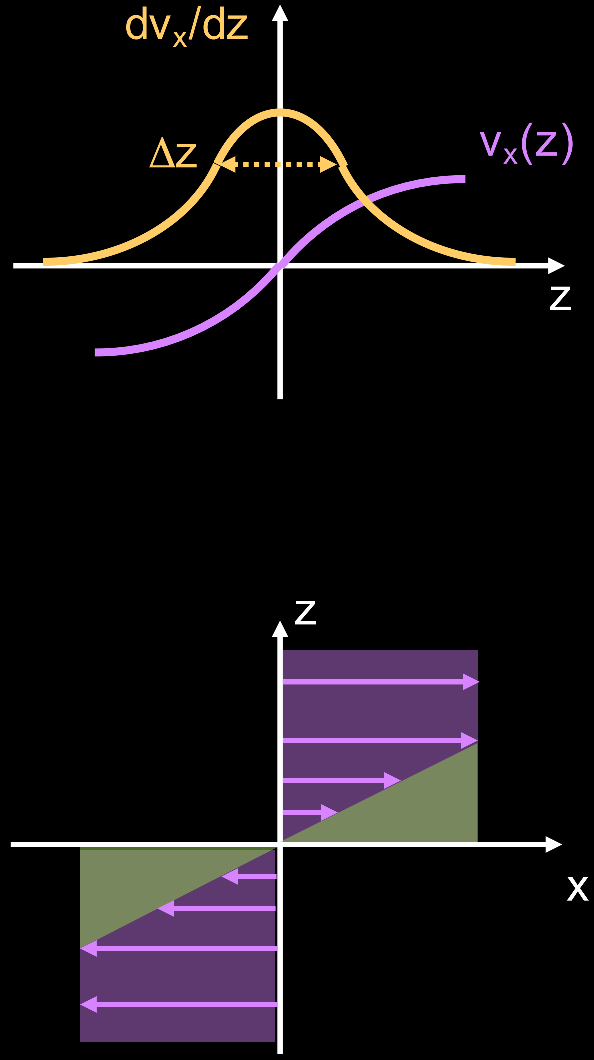

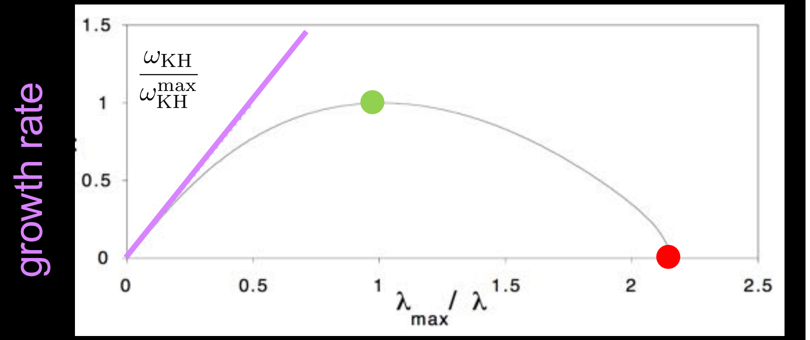

$$(\nabla \times v)_y \equiv \frac{\partial v_z}{\partial x} - \frac{\partial v_x}{\partial z}$$

$$\boxed{\omega_{\mathrm{KH}}^{\mathrm{max}} \sim 0.2\,|\nabla \times v|_{\mathrm{max}}}$$

$$\boxed{\lambda_{\mathrm{max}} \sim 7\,\Delta z}$$

The instability feeds on the kinetic energy gained by smoothing of the velocity profile.

Perturbations with a wavelength shorter than ~3Δz are stable

Loss of large scale power from the growth of parasitic instabilities

Guilet+10

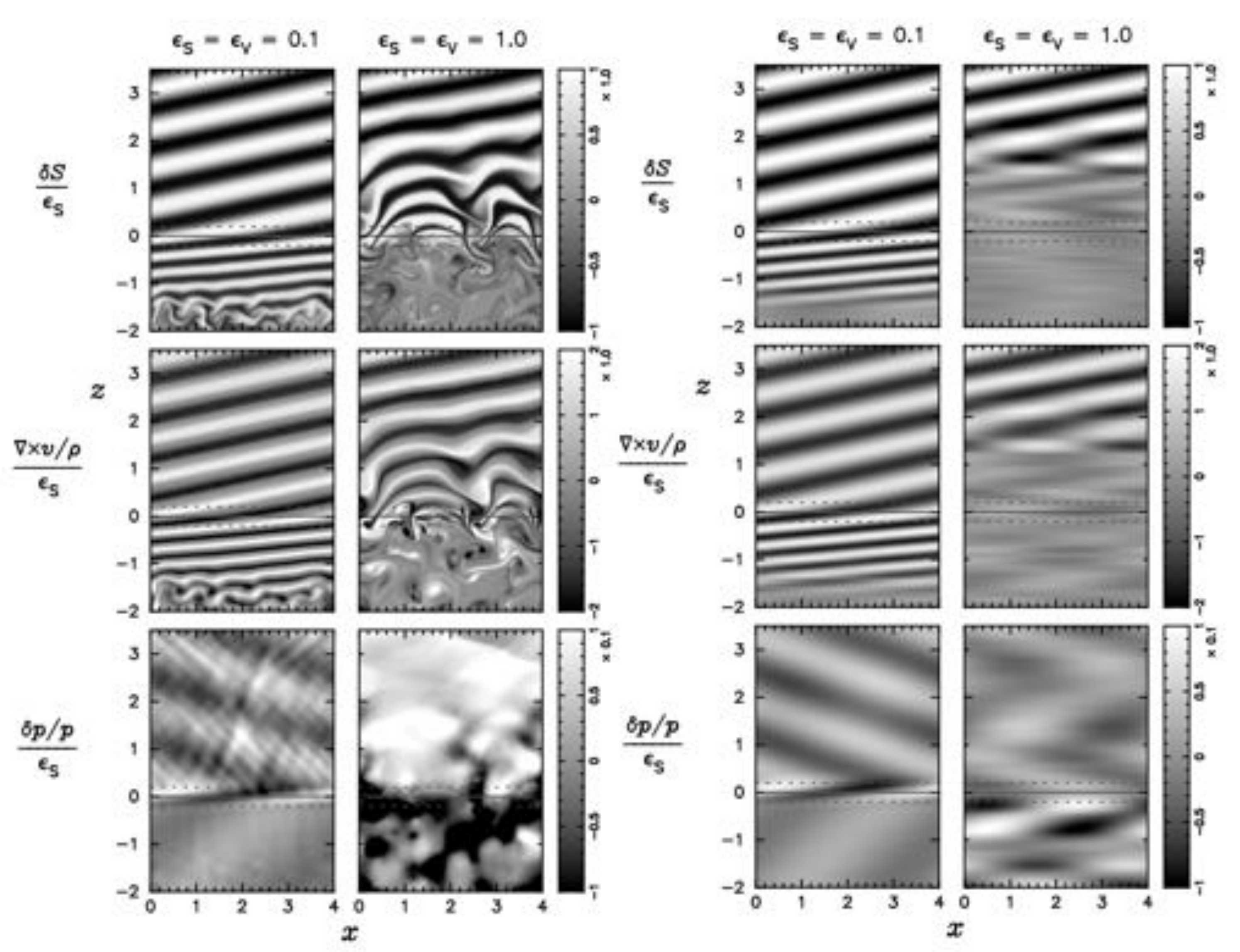

full waves

filtered waves (m_x=1)

From the linear instability mechanism, a short dvection timescale both favours SASI and stabilizes neutrinbo-driven convection (χ<3).

From the non linear saturation mechanism, large SASI amplitudes are expected if the advection velocity is high and if the cooling processes in strong.

The faster the advection, the more difficult the propagation of parasitic instabilities against the flow

The stronger the cooling, the more difficult the destabilisation of the entropy profile by SASI entropy waves

Comparison with numerical simulations

Guilet+10

Fernandez & Thompson 09 (no heating)

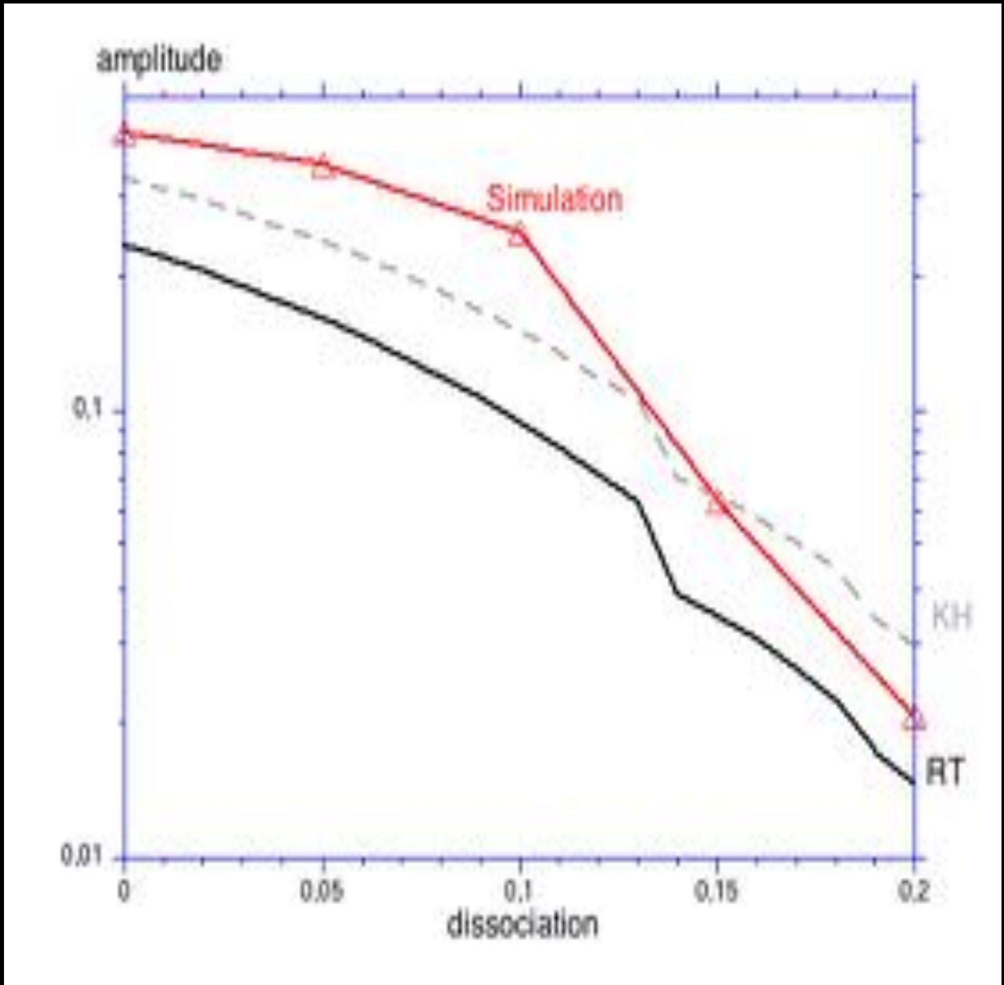

No other saturation mechanism has been proposed since Guilet+10

If neutrino heating increases sufficiently, ν-driven convection is expected to dominate the SASI:

Linearly, the increased thermal pressure makes the flow slower, which is both favourable to convection (increases χ) and makes SASI slower (longer τ_{adv})

Non linearly,
-neutrino heating weakens the stable entropy gradient and allows a faster RT growth of parasites on SASI entropy waves,
-the slower advection velocity also favours the propagation of parasites againt the stream,
-the turbulence driven by small scale convective motions acts as a viscous diffusive process for lage scale SASI waves.

First 3D simulation: redistribution of angular momentum by the spiral mode of SASI

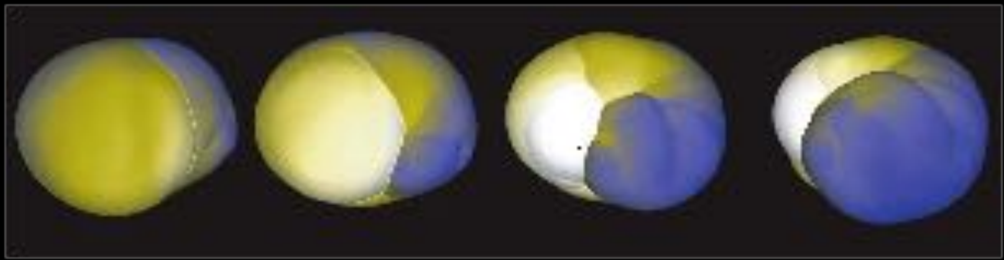

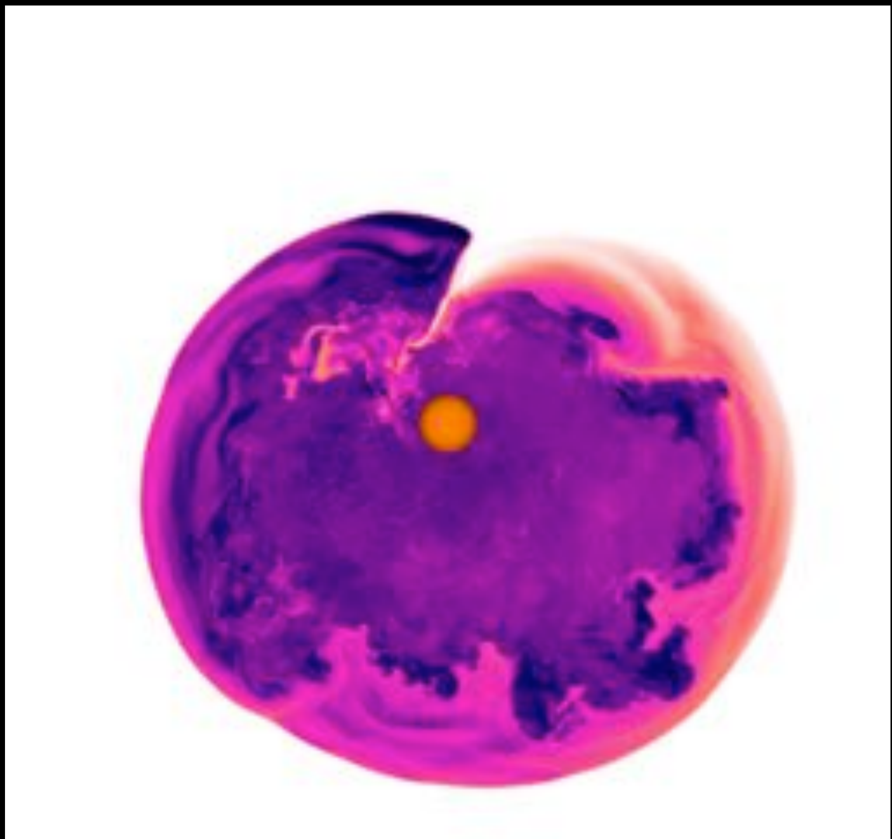

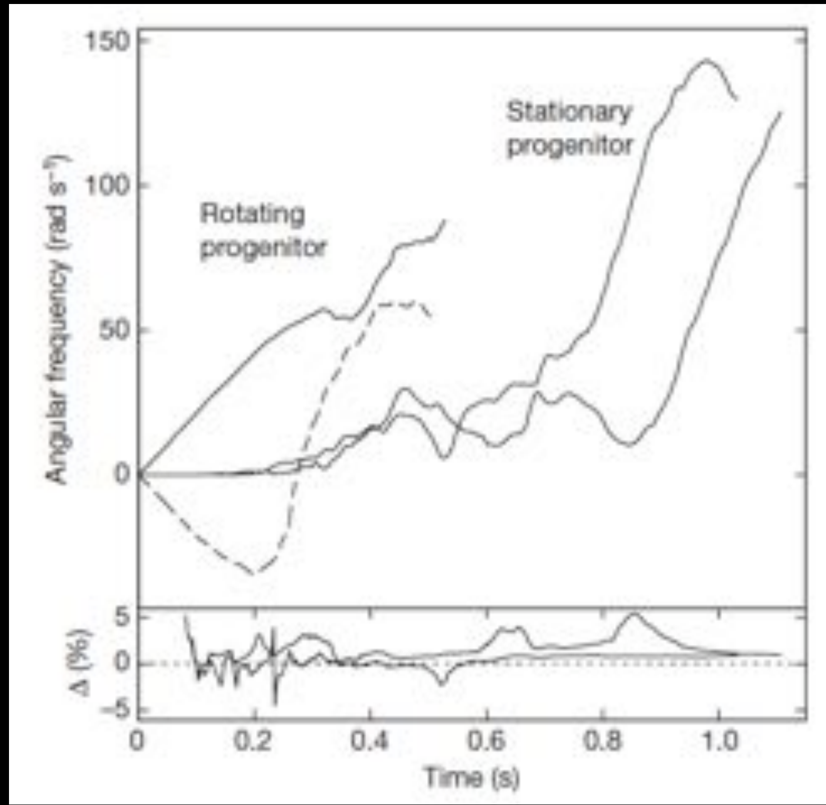

Blondin & Mezzacappa 07

Even if the progenitor is not rotating, SASI is able to spin up the neutron star and the ejecta in opposite directions.

Formal similarity between SASI and SWASI

accretion of gas on a cylinder

density ρ, velocity v, sound speed $c \propto \rho^{\frac{\gamma-1}{2}}$

$$\frac{\partial\rho}{\partial t} + \nabla\cdot(\rho v) = 0$$

$$\frac{\partial v}{\partial t} + w\times v + \nabla\left(\frac{v^2}{2} + c^2\log\frac{\rho}{\rho_0} + \Phi\right) = 0$$ isothermal

$$\frac{\partial v}{\partial t} + w\times v + \nabla\left(\frac{v^2}{2} + \frac{c^2}{\gamma-1} + \Phi\right) = \frac{c^2}{\gamma}\nabla S$$ adiabatic

inviscid shallow water accretion

depth H, velocity v, wave speed $c = (gH)^{\frac{1}{2}}$

$\Phi = gz$

$c^2 = gH$

$$\frac{\partial H}{\partial t} + \nabla\cdot(Hv) = 0$$

$$\frac{\partial v}{\partial t} + w\times v + \nabla\left(\frac{v^2}{2} + c^2 + \Phi\right) = 0$$

- Inviscid shallow water: intermediate between "isothermal" and "isentropic γ=2"

isothermal shock $\mathcal{M}_2 = \frac{1}{\mathcal{M}_1}$

hydraulic jump $\mathcal{M}_2 = \frac{2^{\frac{3}{2}}\mathcal{M}_1}{\left[(1+8\mathcal{M}_1^2)^{\frac{1}{2}} - 1\right]^{\frac{3}{2}}}$

jump conditions: conservation of mass flux and momentum flux: energy is dissipated

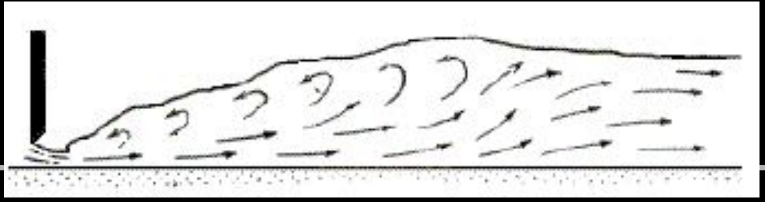

Analogy between hydraulic jumps and shock

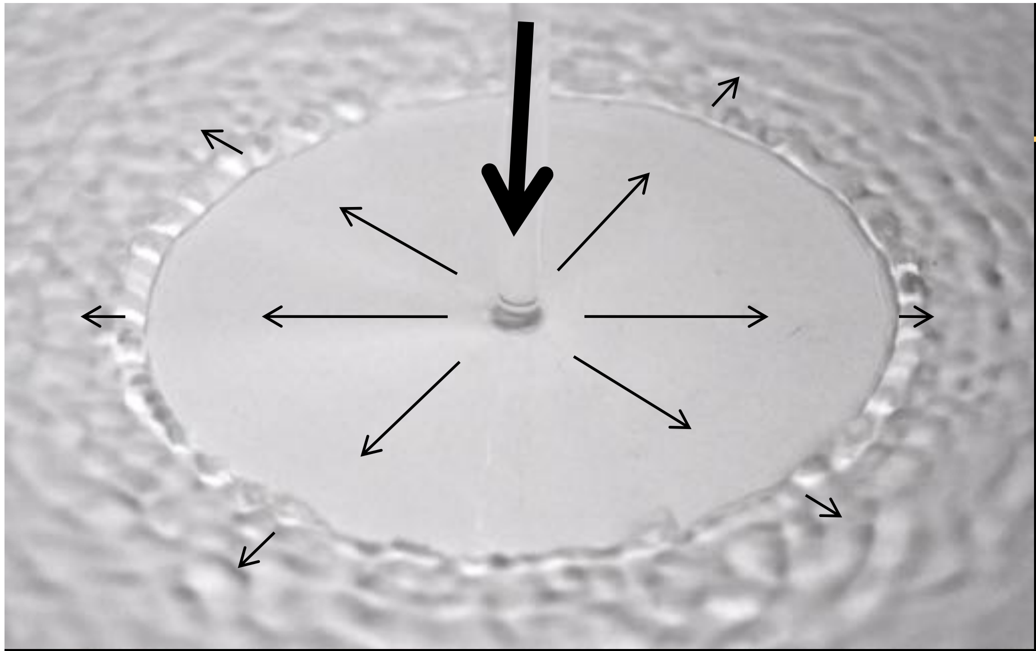

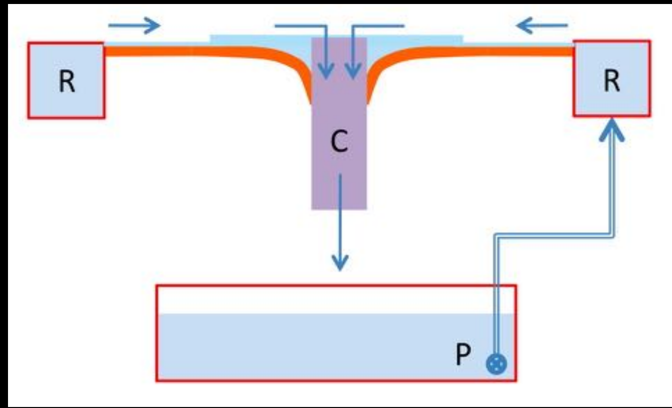

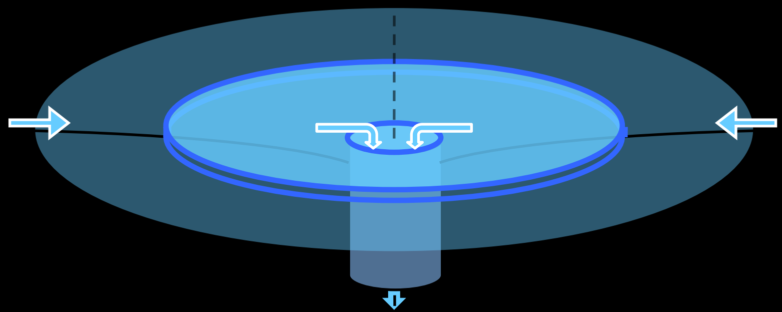

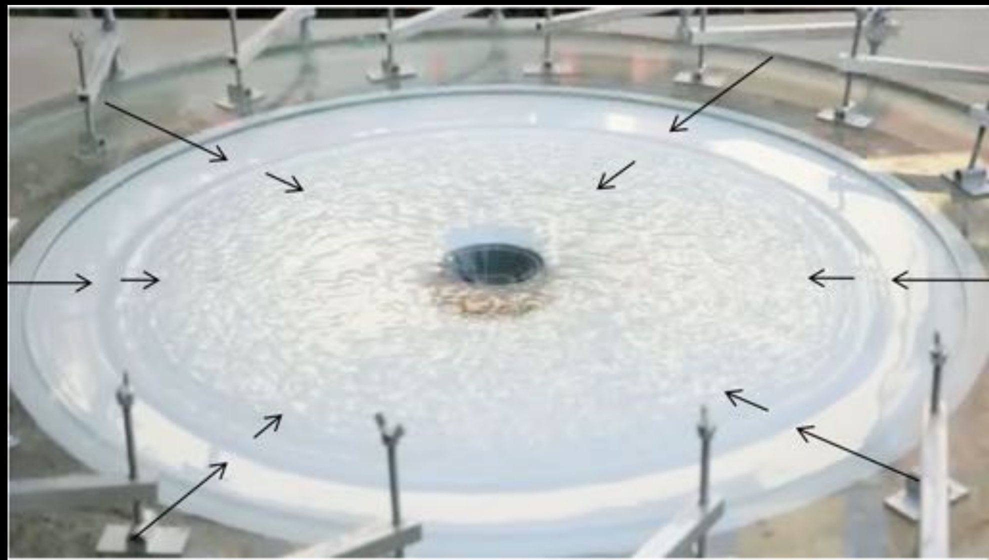

acoustic waves
shock wave
pressure

↔

surface waves
hydraulic jump
depth

Hydraulic jump conditions

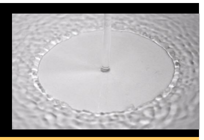

The shallow water flow is also described by 2 physical quantities: velocity and depth (no entropy analogue).
Depth plays the same role as the compressibility of a gas (i.e. surface density).
The jump conditions for a hydraulic jump are deduced from the conservation of mass flux and momentum flux.
Energy is dissipated in a viscous roller within the width of the hydraulic jump.

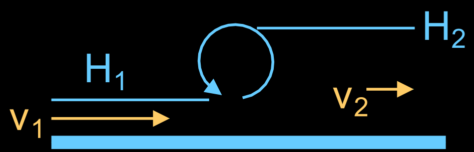

$$H_1 v_1 = H_2 v_2,$$
$$\frac{gH_1^2}{2} + H_1 v_1^2 = \frac{gH_2^2}{2} + H_2 v_2^2.$$

The Froude number is analogous to the Mach number $\mathrm{Fr} \equiv \frac{v}{(gH)^{\frac{1}{2}}}$

$$\mathrm{Fr}_1 H_1^{\frac{3}{2}} = \mathrm{Fr}_2 H_2^{\frac{3}{2}},$$
$$H_1^2(1+2\mathrm{Fr}_1^2) = H_2^2(1+2\mathrm{Fr}_2^2).$$

$$\left(1+2\mathrm{Fr}_1^2\right)\mathrm{Fr}_2^{\frac{4}{3}} = \left(1+2\mathrm{Fr}_2^2\right)\mathrm{Fr}_1^{\frac{4}{3}}$$

This polynomial of order 3 in $\mathrm{Fr}^{3/2}$ can be factorized by $(\mathrm{Fr}_1^{3/2}-\mathrm{Fr}_2^{3/2})$

$$(\mathrm{Fr}_2^{\frac{2}{3}} - \mathrm{Fr}_1^{\frac{2}{3}})(-2\mathrm{Fr}_2^{\frac{4}{3}}\mathrm{Fr}_1^{\frac{4}{3}} + \mathrm{Fr}_2^{\frac{2}{3}} + \mathrm{Fr}_1^{\frac{2}{3}}) = 0$$

$\mathrm{Fr}_2^{3/2}$ is thus a root of a second order polynomial $2\mathrm{Fr}_2^{\frac{4}{3}}\mathrm{Fr}_1^{\frac{4}{3}} - \mathrm{Fr}_2^{\frac{2}{3}} - \mathrm{Fr}_1^{\frac{2}{3}} = 0$

$$\mathrm{Fr}_2 = \frac{1}{8\mathrm{Fr}_1^2}\left[1+(1+8\mathrm{Fr}_1^2)^{\frac{1}{2}}\right]^{\frac{3}{2}}$$

$$\frac{v_2}{v_1} = \frac{H_1}{H_2} = \left(\frac{\mathrm{Fr}_2}{\mathrm{Fr}_1}\right)^{\frac{2}{3}} = \frac{1}{4\mathrm{Fr}_1^2}\left[1+(1+8\mathrm{Fr}_1^2)^{\frac{1}{2}}\right]$$

The jump conditions for hydraulic jumps differ slightly from the gas

For a strong jump: $\frac{v_2}{v_1} \propto 2^{-\frac{1}{2}}\mathrm{Fr}_1^{-1}$, $\mathrm{Fr}_2 \propto 2^{-\frac{3}{4}}\mathrm{Fr}_1^{-\frac{1}{2}}$.

Isothermal shock: $\frac{v_2}{v_1} = M_1^{-2}$, $M_2 = M_1^{-1}$.

SWASI: simple as a garden experiment

May 2010

June 2010

October 2010

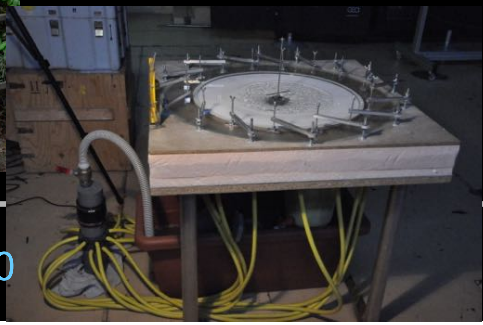

November 2010

CEA Saclay November 2013

Dynamics of water
in the fountain

Dynamics of the gas
in the supernova core

diameter 40cm
3s/oscillation

1 000 000 x bigger
100 x faster

diameter 400km
0.03s/oscillation

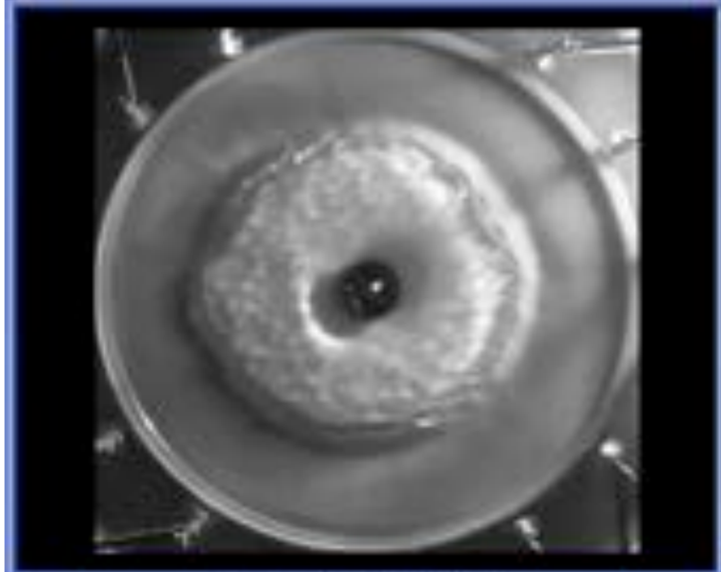

Expérience hydraulique

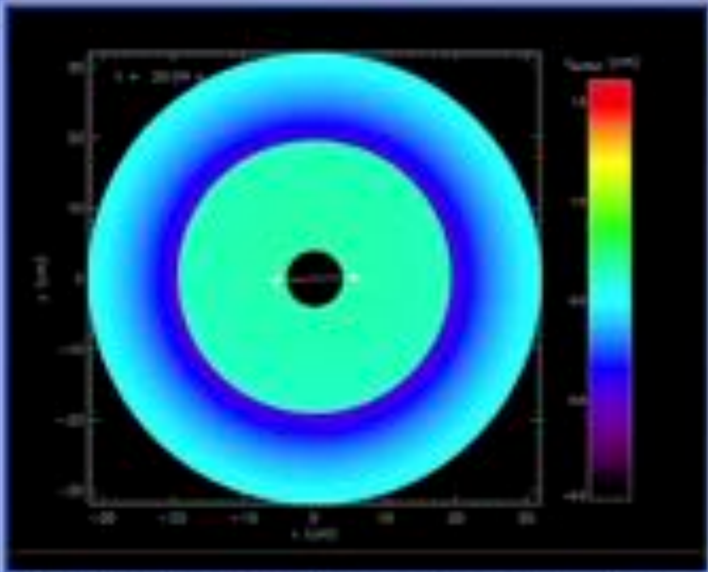

Simulation numérique de l'expérience hydraulique

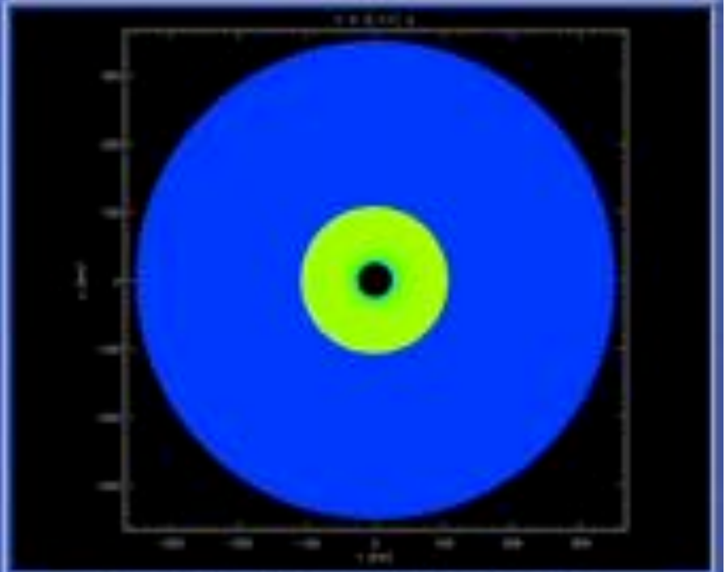

Simulation numérique de l'onde de choc dans le coeur de la supernova

Comparaison to a 2D shallow water model

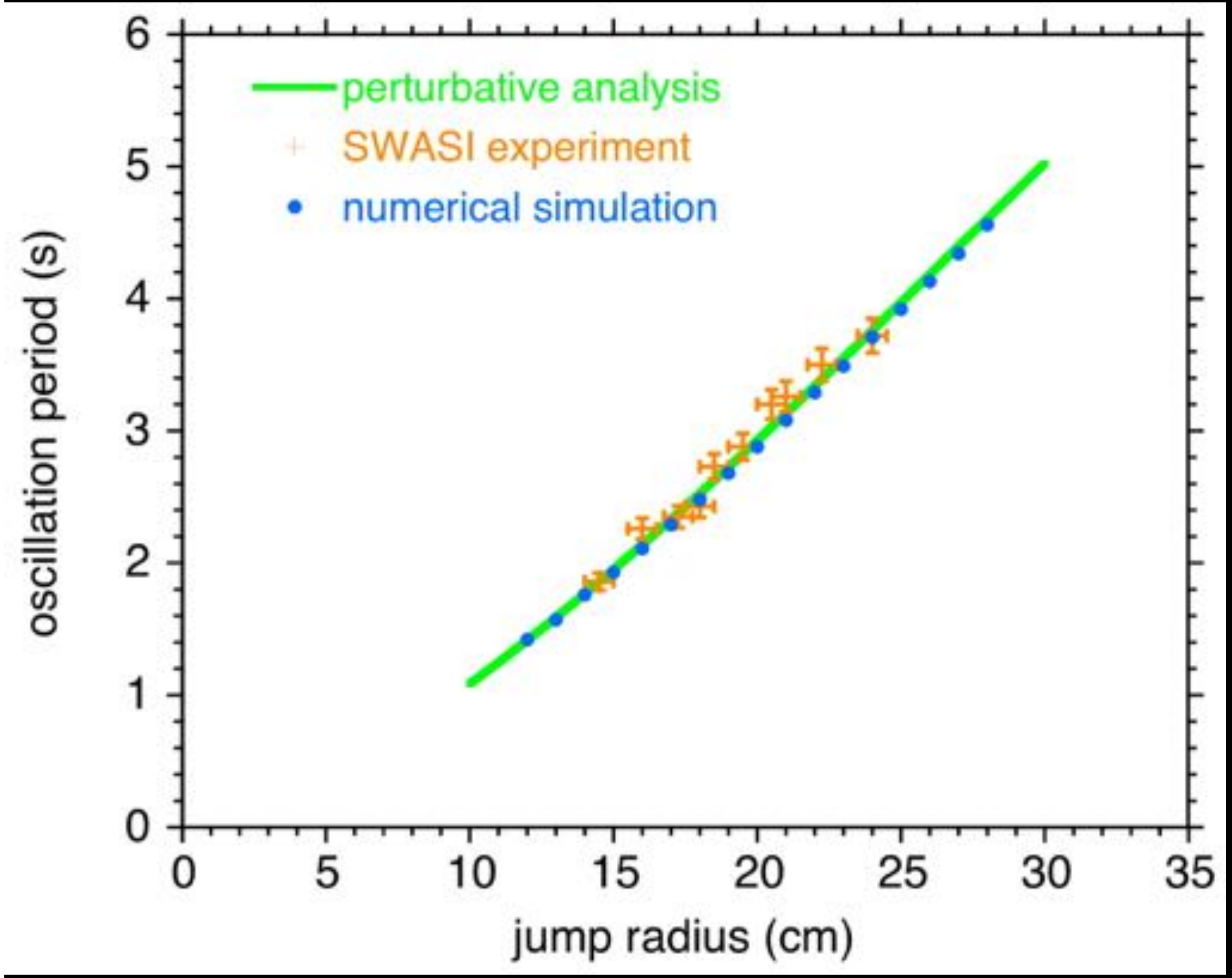

Foglizzo+12

Parameters of the experiment

Foglizzo+12

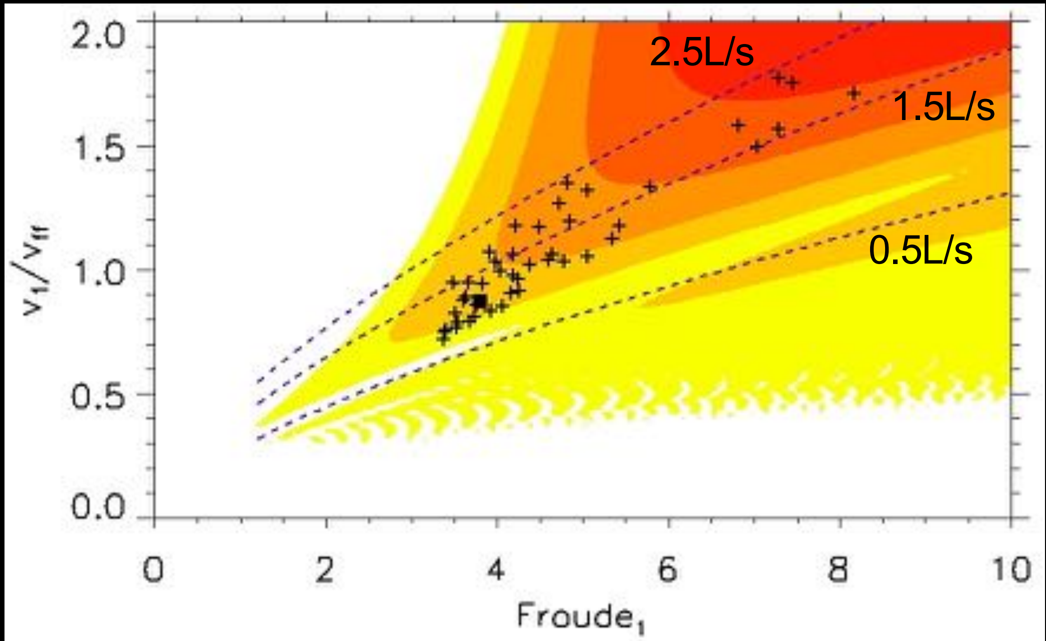

$$v = \frac{Q}{2\pi r H}$$
$$c = (gH)^{\frac{1}{2}}$$
$$v_{\rm ff} \equiv \left(\frac{2gR_\Phi^2}{r}\right)^{\frac{1}{2}}$$

$$\Phi \equiv gH_\Phi(r)$$
$$H_\Phi(r) \equiv -\frac{R_\Phi^2}{r}$$

H_ϕ=5.6cm
R_{inj}=33cm

$$\mathrm{Fr} \equiv \frac{v}{c} = \frac{Q}{2\pi r g^{\frac{1}{2}} H^{\frac{3}{2}}}$$
$$\frac{v}{v_{\rm ff}} = \frac{Q}{2^{\frac{3}{2}}\pi g^{\frac{1}{2}} r^{\frac{1}{2}} H R_\Phi}$$

$$\mathrm{Re} \equiv \frac{Hv}{\nu} = 650\left(\frac{H}{1\mathrm{mm}}\right)^{\frac{3}{2}}\left(\frac{\mathrm{Fr}}{4}\right)\left(\frac{20\mathrm{cm}}{r}\right)$$

at the outer boundary:

-slit size H_{inj} ~ 0.3-1mm
-flow rate Q ~ 0.7-2 L/s
} → (flow velocity & wave speed) → (Froude number & v/v_{ff})

-rotation rate ~0-0.5Hz → angular momentum

at the inner boundary:

-radius of the accretor R_{ns}=4-6cm

-height of the inner cylinder → radius of the stationary jump R_{jp}=15-25cm → R_{jp}/R_{ns}

Advantages and limitations of the shallow water analogy

- simple & intuitive
- explore with an experimental tool
- inexpensive

$$\Phi = gz$$

$$c^2 = gH$$

$$\frac{\partial H}{\partial t} + \nabla \cdot (Hv) = 0$$

viscous drag

$$= -3\nu \frac{v}{H^2}$$

$$\frac{\partial v}{\partial t} + w \times v + \nabla \left(\frac{v^2}{2} + c^2 + \Phi \right) = \cancel{0}$$

product of verticaly averaged velocity or vorticity

γ=2

missing entropy gradient $\frac{c^2}{\gamma}\nabla S$

Theoretical framework:

- 2D slice of a 3D flow
- no buoyancy effects
- γ=2
- accreting inner boundary

Experimental constraints:

- viscous drag
- turbulent viscosity
- approximately shallow water
- vertical velocity profile
- hydraulic jump dissipation 3<Fr<8

The inner boundary condition in the shallow water model

The inner boundary is modelled as a critical point of transition from Fr<1 to Fr>1

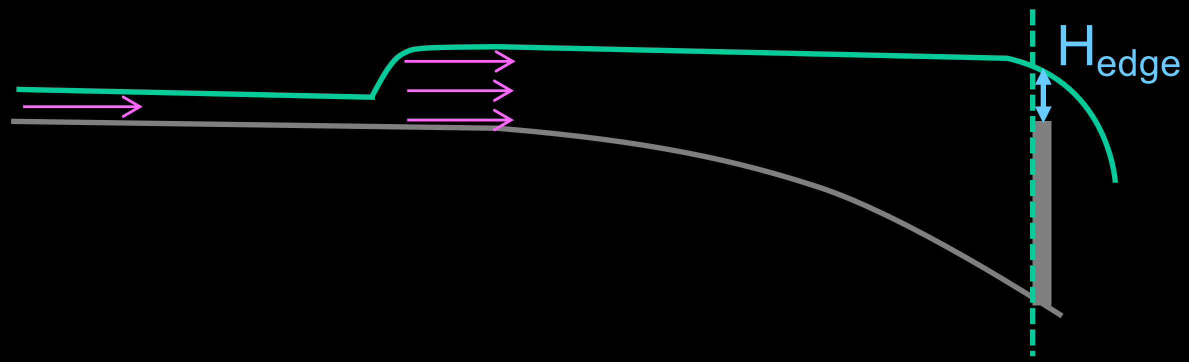

$$2\pi r_{\rm ns} H_{\rm edge} |v_{\rm ns}| = Q,$$
$$v_{\rm ns}^2 = g H_{\rm edge}.$$

The boundary condition can be written immediately ahead of the inner cylinder using the regularity conditions required by the pertrubative equations at the critical point Fr=1 and using the continuity of the energy density δf and the mass flux δh.

$$\frac{\mathrm{d}\delta f}{\mathrm{d}r} = \frac{i\omega v_r}{1-\mathrm{Fr}^2}\left(\delta h - \frac{\delta f}{c^2}\right) + \frac{\bar{\nu} v_r}{H^2(1-\mathrm{Fr}^2)}\left[3\frac{\delta f}{c^2} - (1+2\mathrm{Fr}^2)\delta h\right],$$
$$\frac{\mathrm{d}\delta h}{\mathrm{d}r} = \frac{i\omega}{v_r(1-\mathrm{Fr}^2)}\left(\frac{\delta f}{c^2} - \mathrm{Fr}^2\delta h\right) - \frac{im}{r^2 v_r} r\delta v_\theta,$$
$$\frac{\mathrm{d}r\delta v_\theta}{\mathrm{d}r} = \frac{imv_r}{1-\mathrm{Fr}^2}\left(\delta h - \frac{\delta f}{v_r^2}\right) + \left(\frac{i\omega}{v_r} - \frac{\bar{\nu}}{v_r H^2}\right) r\delta v_\theta$$

$$\delta f(r_{\rm ns}) = v_{\rm ns}^2 \delta h(r_{\rm ns})$$

Beyond the shallow water approximation: phase mixing of dragged vorticity ?

$$\mathrm{Re}_H \equiv \frac{Hv}{\nu} = 796\left(\frac{Q}{1\mathrm{L/s}}\right)\left(\frac{20\mathrm{cm}}{R_{\mathrm{jump}}}\right) = 2650\left(\frac{Q}{1\mathrm{L/s}}\right)\left(\frac{6\mathrm{cm}}{R_{\mathrm{NS}}}\right)$$

$$\mathrm{Re}_L \equiv (R_{\mathrm{inj}} - R_{\mathrm{jump}})\frac{v_{\mathrm{inj}}}{\nu} = 10^5\left(\frac{Q}{1\mathrm{L/s}}\right)\left(\frac{0.6\mathrm{mm}}{H_{\mathrm{inj}}}\right)$$

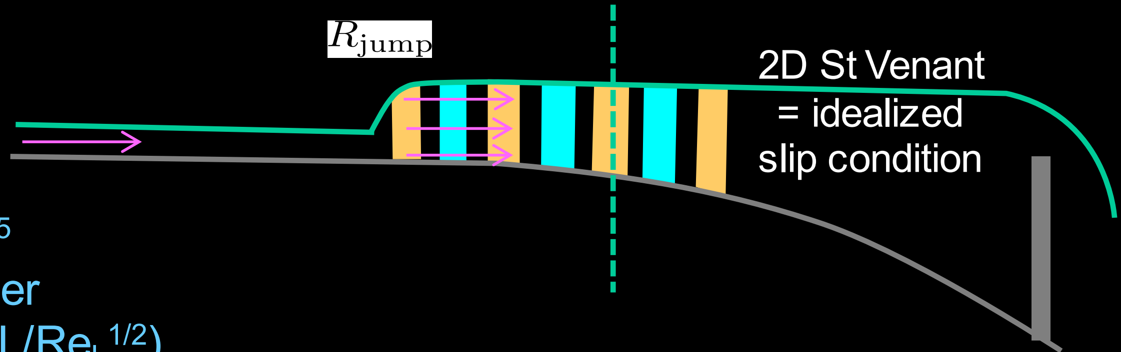

ill-defined vertical structure H(R)

- laminar/turbulent transition $\mathrm{Re}_L \sim 5\times10^5$
- vertical extension of the boundary layer
  - $\delta_{jp} \sim 2$mm if laminar ($4.91\ L/\mathrm{Re}_L^{1/2}$)
  - $\delta_{jp} \sim 5$mm if turbulent ($0.38\ L/\mathrm{Re}_L^{1/5}$)

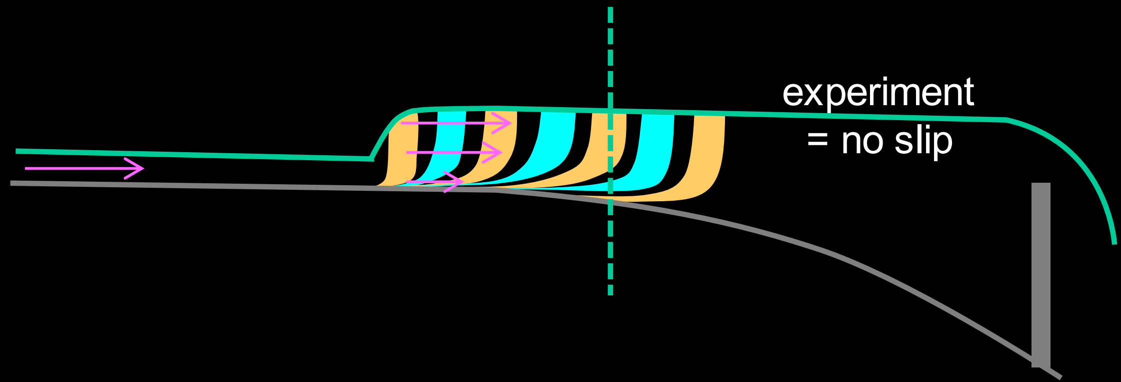

reference examples

- half-Poiseuille: $\frac{v(z)}{<v>} \sim \frac{3z}{2H}\left(2 - \frac{z}{H}\right)$
- turbulent prescription: $\frac{v(z)}{<v>} \sim \frac{8}{7}\left(\frac{z}{H}\right)^{\frac{1}{7}}$

The vertically averaged vorticity is damped by a factor Q

$$Q \sim \int_0^H \frac{\mathrm{d}z}{H}\cos\left[\frac{\omega_{\mathrm{SASI}}\Delta R}{v(z)}\right] \begin{array}{l}\sim 0.27\ \text{(laminar)}\\ \sim 0.52\ \text{(turbulent)}\end{array}$$

Counter spinning inner regions

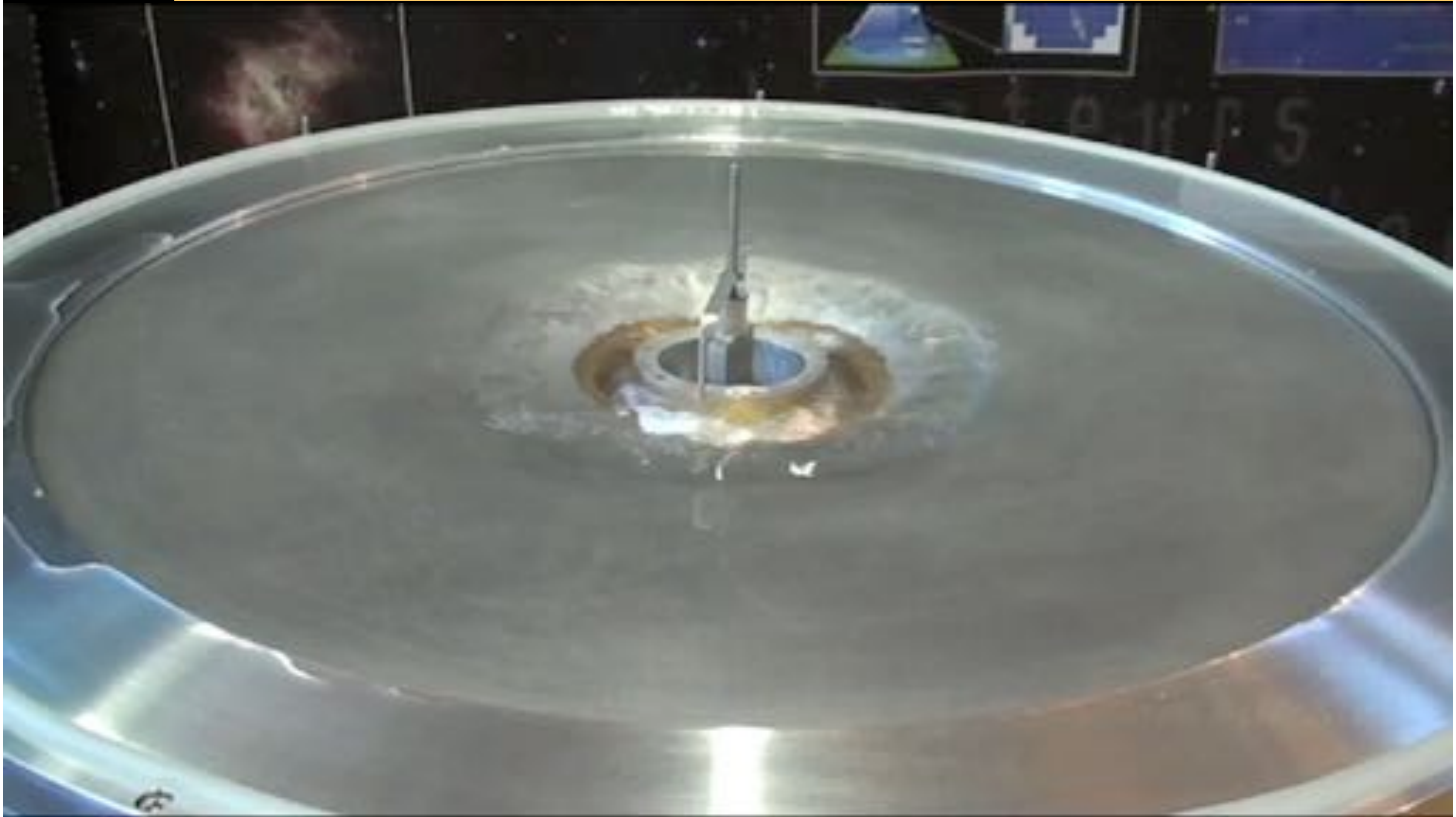

The spin up uf the neutron star induced by the spiral mode of SASI

Kazeroni+17

Cylindrical stationary accretion, neutrino cooling mimicked by a cooling function

-the strength of SASI increases with the radius ratio $R = r_{sh}/r_{ns}$

-unexpected stochasticity and possible change in the direction of rotation

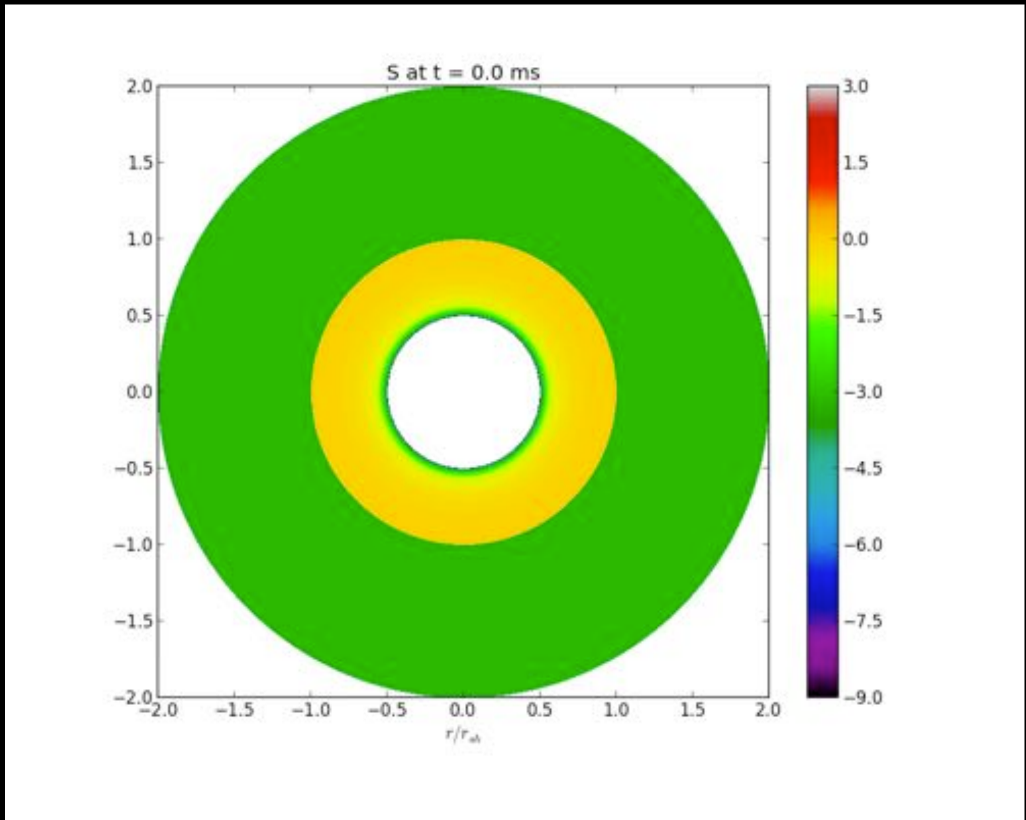

$r_{sh}/r_{ns} = 2$

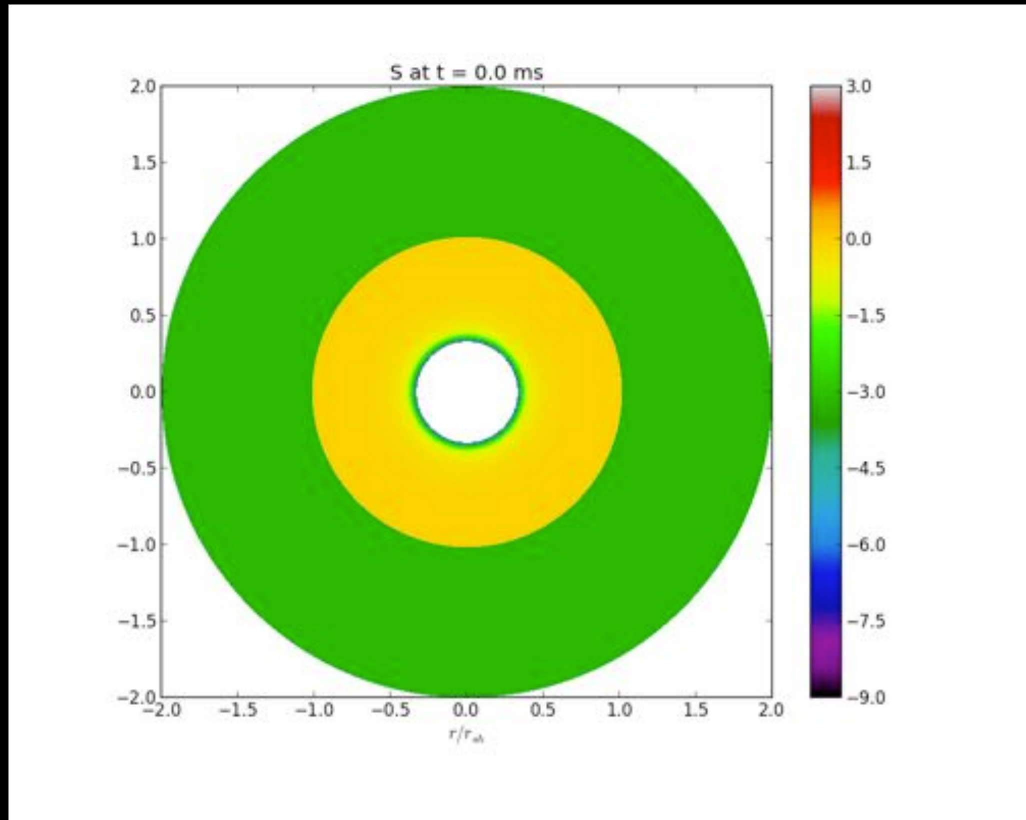

$r_{sh}/r_{ns} = 3$

Pulsar spin from a non rotating progenitor (Guilet & Fernandez 14)

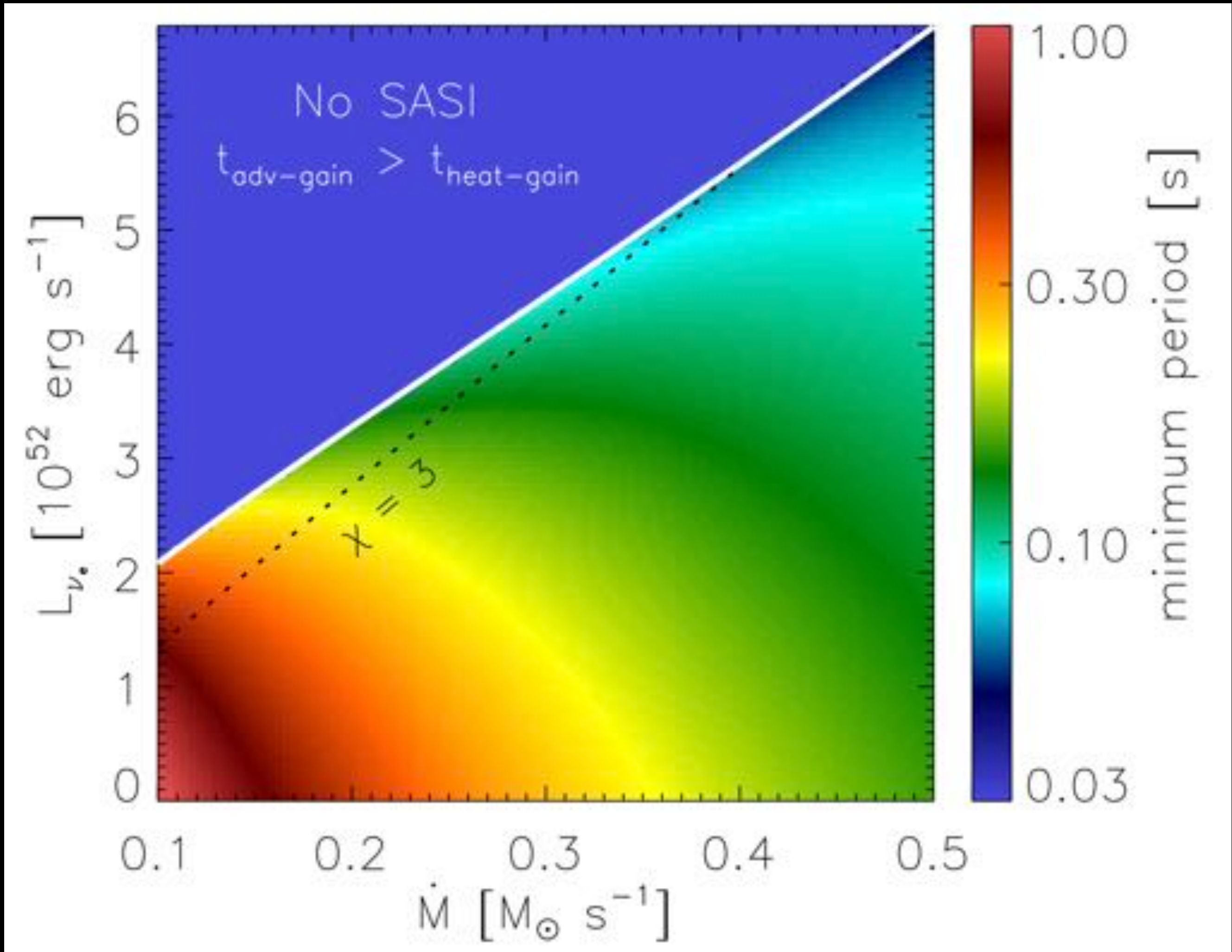

The density of angular momentum captured in the SASI spiral wave can be related to the amplitude Δr of the saturated mode.

$$\frac{l}{\dot{M} r_{\rm sh}} \sim m \frac{\omega_r r_{\rm sh}}{2\pi v_{\rm sh}} \left(\frac{\Delta r}{r_{\rm sh}}\right)^2$$

The resulting distribution of rotation periods of pulsars born from a non rotating progenitor through a SASI dominated explosion is comparable to the slowest part of the distribution of pulsar periods >80ms

Towards higher Reynolds numbers

Foglizzo & Durand 17

-diameter 3m50: Reynolds x 10
→ less viscous, more turbulent

-overflowing injection
→ "free fall"